We would like to thank referee #1 for the valuable and constructive comments. We address all comments (in italic bold) and specify the position of the proposed updated text.

Comment 1
My major concern is that the parameterization has been tuned and validated for the same wind farm (Section 4.1.1). Results herein presented are therefore a maximum limit on the performance of the scheme. Ideally you should calibrate the parameterization on an independent wind farm. If this is not possible you should show results of the sensitivity simulations you performed to select the parameter of the parameterization, σ_0.

The reviewer is right that ideally the initial length scale should be determined from the measurements at an independent wind farm. Unfortunately, we don't access long-term measurements from other wind farms. As stated in the text, we have tried to use the available observations in an as independent manner as possible:
1) we use the turbine data that represents a rotor swept area averaged wind speed to determine the initial length scale σ_0. Then, we use point measurement met mast wind speeds at $2\,\text{km}$ and $6\,\text{km}$ downstream for the validation. 2) the wind farm data and the met mast data are from two different sub-sets, since they have different filter criteria (turbine measurements have the additional requirement that they are only selected when up-stream turbines are operation). 3) The initial length scale has been determined from one wind speed bin ($9\,\text{m/s}$), whereas we validated the scheme for five wind speed bins.

As proposed by the reviewer, we have updated Fig. 4, which now shows the sensitivity of the initial length scale within the wind farm. The plot has been attached at the end of the document (incl. updated caption). Related to the Fig. 4, we propose the following change on p. 3495 l. 20–21:

> Figure 4 shows the results from the simulations with $\sigma_0 = 1.7\,R_0$, which had the smallest overall bias compared to the measurements.

to:

> The lines in Fig. 4 show the results from the simulations with $\sigma_0 = 1.7\,R_0$, which had the smallest overall bias compared to the measurements. Additionally, the coloured dots indicate the sensitivity to the initial length scale for $\sigma_0 =$ 1.5 and 1.9 R_0.

Comment 2
Having the scheme tuned for this particular wind farm somewhat hampers the comparison with the WRF-WF parameterization that has not been tuned for this particular wind farm. This should be clarified.

1

As has been mentioned in the previous comment, the EWP scheme uses the initial length scale, σ_0, that has been tuned by the measurements inside the Horns Rev I wind farm. The WRF-WF scheme on the other hand has no free parameters. Their drag force depends on the turbine specific thrust curve and the additional turbulence on the difference between the thrust and power curve (Eq. 16 on p. 3496 l. 7). Therefore, it was remarkable that the velocity at hub-height was almost identical in the EWP and WRF-WF scheme at the end of the wind farm (although the structure of the velocity profiles differed). The validation was performed in the wake recovery of the wind farm were the schemes are not active anymore.

To clarify that the WRF-WF scheme has no tunable constants, we propose to change on p. 3496 l. 23:

> This approach is used in the experiments performed in Sect. 5.

to:

> In Sect. 5, we use the up-dated WRF-WF parametrisation from WRFV3.6. Its input parameters, the power and thrust curve, come from the Vestas V80 turbine.

Also, we would mention more explicitly in the introduction of section 5 on p. 3497 l. 1–6 that the EWP scheme uses a calibrated initial length scale from the wind farm data and change:

> To obtain a complete picture of the modelled velocity field within and downstream of the Horns Rev I wind farm, we compare the hub-height velocity simulated by the WRF model using the two wind farm parametrisations for one wind speed bin. We used the second most frequently observed wind speed bin (10 m s^1), which is different from that used in the calibration (Sect. 4.1.1), to be as calibration independent as possible. Afterwards, we compare the modelled velocities for all wind speed to the measurements at M6 (2 km downstream) and M7 (6 km downstream).

to:

> To obtain a complete picture of the modelled velocity field within and downstream of the Horns Rev I wind farm, we compare:
> (I) the hub-height velocity simulated by the WRF model using the two wind farm parametrisations for the $10 \, \mathrm{m\,s^{-1}}$ wind speed bin. We recall that the initial length scale of the EWP scheme has been determined at $9 \, \mathrm{m\,s^{-1}}$.
> (II) the modelled velocities to the measurements at M6 (2 km downstream) and M7 (6 km downstream) for all five wind speeds (7, 8, 9, 10, and $11 \, \mathrm{m\,s^{-1}}$).

In the discussion, we propose to add the here underlined text on p. 3503 l. 18–22:

Before we validated the results of the schemes in the wake of the wind farm, the a priori unknown initial length scale of the EWP scheme had to be determined. We did this using the turbine power measurements from the most frequently observed wind speed bin. This limitation could not be avoided, since to our knowledge no other long-term measurements from large offshore wind farms were available. On the other hand, for the WRF-WF scheme we have used the turbine specific thrust and power curves, which are its only input parameters.

Comment 3
Finally, it seems the authors have available a large observational dataset but have restricted the comparison for westerly winds with different atmospheric conditions. If possible, the authors should extend the validation showing more specific results of the parameterizations performance (e.g. wind farm wakes as a function of the hub height wind speed). I do not see a major reason for not including a more extended comparison having the data and the simulations available.

As discussed in section 3, the met masts that have been used in the validation are located to the East of the Horns Rev I wind farm. Therefore, wind farm wakes can only be captured at the met masts when the wind blows from the west.
For this wind direction sector, we used all wind speeds between $7\,\mathrm{m/s}$ (to be above the cut-in wind speed of 4 m/s in the entire wind farm) and $11\,\mathrm{m/s}$ (to be below the wind speed were pitch control starts, $13\,\mathrm{m/s}$). In Fig. 5, we show the downstream velocity recovery for the $10\,\mathrm{m/s}$ wind speed bin. Then, Fig. 6 compares for all selected wind speed bins (7, 8, 9, 10, and 11 m/s), the modelled wind speed at the met masts to that of the measurements. Therefore, figures similar to Fig. 5 for additional wind speeds would not provide any additional information, since Fig. 6 shows the recovery for all wind speed bins.

SPECIFIC COMMENTS

1. Page 3485, Line 12: it will be good if you can describe the ensemble-average methodology, its differences with the more standard approach of volume averaged shown in Fig. 1, and why is relevant for the EWP wind farm parameterization.

The description of the averaging is an important part of the paper, we propose therefore to update section 2.2 and Fig. 1. To support the description of the averaging procedure in more detail we have prepared an additional Appendix (attached).

1) In the new Appendix, we would adapt the notation of Raupach and Shaw (1982) for the double averaging. For consistency, we would change to this notation in the whole paper. Therefore, we propose to substitute on p. 3485 l. 11–12:

> We will use the notation and symbols of Wyngaard (2010). The upper-case letters refer to ensemble-averaged quantities, whereas lower-case letters refer to fluctuations.

with:

> We use an over-line to denote ensemble-averaged quantities and a prime for a fluctuation around the ensemble average.

2) Regarding the averaging, we have edited Fig. 1 (attached below) and we propose to substitute on p. 3486 l. 12–21:

> The previously defined variables in the Eqs. (1) and (3) have to be redefined on the three-dimensional model grid. A new volume-averaged velocity equation is derived by integrating Eq. (1) over the grid-cell volume. For Eq. (3), we define a (random) velocity fluctuation at any hypothetical measurement point within a grid-cell volume to be the difference between the ensemble-averaged and the instantaneous velocity. This is illustrated schematically in Fig. 1a. Then, the grid-cell averaged TKE can be thought of as the variance of the velocity fluctuations around the ensemble-averaged velocity and not around the grid-cell averaged velocity as shown in Fig. 1b.
>
> The aim is to obtain expressions for the terms P_t (Eq. 3) and F_D (Eq. 1) that are consistent with the mesoscale model flow equations. The expression for Pt can be found by multiplying the NavierStokes equations with the velocity fluctuation and then applying Reynolds averaging. This gives for the additional source term:
>
> $$P_\mathrm{t} = \overline{\rho\, A_\mathrm{r}\, c_\mathrm{T}\, (U_i + u_i)^2\, u_i}/2 \sim \rho\, A_\mathrm{r}\, C_\mathrm{T} U \overline{u_i^2}, \tag{4}$$
>
> where $\rho\, A_\mathrm{r}\, c_\mathrm{T}\, (U_i + u_i)^2$ is the instantaneous forcing due to the action of the wind turbine, the lower case c_T the instantaneous thrust coefficient, the upper case C_T the averaged thrust coefficient, and Ar the rotor area.

4

with:

The previously defined variables in the Eqs. (1) and (3) have to be redefined on the three-dimensional model grid. We use angle brackets to denote the volume average. The aim is to obtain expressions for the terms $\langle \overline{f_d} \rangle$ and $\langle \overline{p_t} \rangle$ for the wind farm parametrisation that are consistent with the mesoscale model flow equations.

A new volume-averaged velocity equation is derived by integrating Eq. (1) over the grid-cell volume. This gives the expression for $\langle \overline{f_d} \rangle$, which is derived in the following section 2.2.1.

The derivation of the source term $\langle \overline{p_t} \rangle$ depends on the definition of the velocity perturbation. Formally, a velocity perturbation is the difference between the instantaneous and ensemble-averaged velocity. For homogeneous flows, the spatial-averaged velocity can be used for the definition of a velocity fluctuation, since the ensemble average can be approximated by the spatial average. However, the flow around wind turbines is non-homogeneous and consequently the spatial and ensemble average deviate. This has been illustrated in Fig. 1. Double averaging (ensemble and spatial) allows to separate the total kinetic energy into three contributions. Then, the source term $\langle \overline{p_t} \rangle$ in the TKE equation depends on the definition of mean and turbulence kinetic energy. In Appendix A, we discuss in more detail the double averaging and the ways mean and turbulence kinetic energy can be described.

In the EWP scheme, we follow Raupach and Shaw (1982) and Finnigan and Shaw (2008) and define a turbulence fluctuation around the ensemble mean (Approach I in Appendix A). With this definition, we include only the random motion in the TKE. The expression for the volume-averaged $\langle \overline{p_t} \rangle$ can then be found by multiplying the Navier-Stokes equations with the velocity fluctuation and then applying Reynolds averaging. This gives for the source term:

$$\langle \overline{p_t} \rangle = \langle \overline{u_i' f_i'} \rangle \approx -\frac{1}{2} \rho A_r c_{\mathrm{t}} \langle \overline{u_{i,h}^2 u_{i,h}'} \rangle \approx -\rho A_{\mathrm{r}} c_{\mathrm{t}} \langle \overline{u_{i,h} u_{i,h}'^2} \rangle, \tag{4}$$

where $\rho A_r c_{\mathrm{t}} u_{i,h}^2/2$ is the instantaneous forcing due to the action of the wind turbine, c_t the thrust coefficient, A_r the rotor area, and h the turbine hub-height.

3) Because of the changed Fig. (1) and the additional Appendix A, we propose furthermore to up-date on p. 3496 l. 12–14 in Sect. 4.1.2:

The same result, $P_{t,\mathrm{WRF\text{-}WF}} = \rho A_{\mathrm{r}} C_{\mathrm{T}} a \overline{u}^3/2$, can also be obtained by defining a velocity fluctuation as the difference between the grid-cell averaged velocity and the instantaneous velocity as illustrated in Fig. 1b.

to:

The same result, $\langle \overline{p_{t},\text{WRF-WF}} \rangle = \rho A_{\text{r}} c_{\text{t}} a \langle \overline{u} \rangle^3 / 2$, is also obtained by defining a velocity fluctuation as the difference between the grid-cell averaged velocity and the instantaneous velocity (Approach II in Appendix A). In Fig. 1, we illustrated a wake and the difference between the grid-cell averaged velocity (red line) and the instantaneous velocity (grey line) is denoted by u''.

2. Page 3487, lines 5-10: If I understood correctly, the turbulence induced by the rotor is dissipated within the grid cell and Pt is neglected on Eq. 3. This probably has implications for the maximum horizontal resolution that can be achieved by the parameterization. Is there any theoretical/empirical limit?

As the second referee pointed out in his fourth comment, Eq. (4) should have a minus sign. This term would therefore be a sink of TKE. This has no implications on the results, since we have neglected the additional term in Eq. (4).

3. It is not clear to me what are the final equations that are implemented on the WRF model. I think the parameterization only needs to incorporate equations 14 and 15 in the model. Is this correct?

The reviewer is correct that Eqs. (14) and (15) apply the turbine induced drag force to the model's RANS equation. Additionally, Eq. (12) is implemented to determine the effective length scale of the vertical wake extension.

We propose to replace on p. 3491 l. 2–3:

> For each turbine a thrust force is calculated with Eqs. (14) and (15). The total thrust force for a turbine containing grid-cell is then obtained from a superposition of the single turbine thrust forces and is added to the numerical approximation of Eq. (1).

with:

> In the numerical model, Eqs. (14) and (15) are added to the numerical approximation of Eq. (1). Furthermore, Eq. (12) is used to determine the effective length scale σ_e of the vertical wake extension. At every time-step the total thrust force within a grid-cell is obtained from a superposition of the single turbine thrust forces.

as well as on p. 3491 l. 12–13:

> A practical description of how to use the EWP scheme in the WRF model is given in Sect.

with:

A practical description of how to use the EWP scheme in the WRF model is given in the section "Code availability" at the end of the paper.

4. page 3491, line 11: WRF does not have 2nd order PBL closures.

In the revised manuscript we would substitute on p. 3491 l. 11:

second order $\rightarrow$ 1.5 order

5. Page 3493, line 14, is there any specific reason to select the horizontal resolution of 1120m? Why not just 1 km?

This value was chosen to accommodate the uniform spacing of the turbines in the Horns Rev I wind farm. The turbine spacing is 560 m in the West-East direction. Consequently, with a 1120 m horizontal grid-spacing, we obtain in the flow direction a constant number of turbines per grid-cell within in wind farm. In the cross-stream direction, we have defined only one turbine row in the most northern and southern grid-cell, since these rows were not included in the row averaging in the measurements (p. 3495 l. 10–11).

We propose to add the here underlined sentence to p. 3493 l. 14:

$\dots \Delta$ x $= \Delta$ y $= 1120$ m. This horizontal grid-spacing, which is twice the turbine separation, guarantees a constant number of turbines per grid-cell in the flow direction. Equally to the Horns rev I wind farm $\dots$

6. Page 3494, line 11, It is not clear how do you impose the wind speed at the hub height. You mention that you integrate the model for four days and use the resulting wind profile to initialize the wind farm simulations. How do you get the hub height winds that you want to impose?

In the idealised case studies the model is initialised with a constant geostrophic wind. During the simulation period a logarithmic profile develops within the boundary layer. To be certain that the wind speeds converge to a given value, we performed a 4 day simulation for every wind speed and wind direction. For every simulation, we impose a geostrophic wind such that after the entire simulation period of 4 days the hub-height wind speed and the wind direction correspond to the measurement binned values. We found the right geostrophic wind by conducting several experiments. The atmospheric state of that instance is used as a restart file for the wind farm and the background simulation without wind farm, such that all necessary variables for the initialisation of the model are saved. Although the atmospheric state converged after 4 days, we still performed the background

simulation to account for the small oscillations around the steady state ($\pm 0.02\,\mathrm{m/s}$).

In the revised manuscript, we propose to add the here underlined sentence on p. 3494 l. 11:

> ...The atmospheric state of each of these 135 simulations was used to drive: a control simulation without wind farm parametrisation, a simulation with the WRF-WF scheme, and a simulation with the EWP scheme. <u>We used the restart option in the WRF model to initialise these simulations.</u> Each control or wind farm simulation lasts one day, resulting in a total simulation length of five days. The wind speeds in the control simulations were 7, 8, 9, 10, and 11 $\mathrm{m\,s^{-1}}$ at 70 m (hub-height) after 5 days of simulation. <u>We found the right geostrophic wind by conducting several experiments.</u> ...

7. How do you represent the turbulent fluxes at the surface (i.e. sensible heat, latent heat and momentum?) in the idealized experiments?

The atmosphere in the idealised case simulations is dry (p. 3494 l. 4). The surface heat flux was set to zero (p. 3493 l.19). Therefore, the slightly stable initial atmosphere converged to a completely neutral atmosphere (p. 3494 l. 6). The momentum flux is determined by the mynn_surface layer scheme. We defined a constant roughness length of $0.0002\,\mathrm{m}$ for the whole domain and all points represent water (p. 3493 l. 20–21). Consequently, the friction velocity is determined by the mynn_surface layer scheme from the Charnock formula. All the initial profiles and namelist options are included in the link to the available code at the end of the article.

We propose to change on p. 3493 l. 20:

> The surface roughness was constant in time and set to $z_0 = 2 \times 10^{-4}\,\mathrm{m}$ for the entire domain.

to:

> The domain is fully contained over water and it had a constant roughness length of $z_0 = 2 \times 10^{-4}\,\mathrm{m}$ in time, which follows the WMO standards. The friction velocity is obtained with the Charnock formula.

and add to Table 2:

Surface layer scheme:	MYNN Monin-Obukhov similarity theory (option 5)
TKE advection:	Yes
Roughness length (m):	2×10^{-4}

8. Page 3494, line 17. Are the simulated wind speeds stable enough to use only the instantaneous wind speed in the validation? Usually you average results over a certain temporal period.

All simulations have reached a steady state and therefore it is not necessary to average over time. The amplitude of the oscillations in wind speed at hub-height was less than $0.02\,\mathrm{m/s}$ for the final day.

In the revised manuscript we would explicitly mention that we use the converged wind speed and propose to add the here underlined part of the sentence to p. 3497 l. 12–13:

> In the validation, we use the instantaneous model outputs from the converged flow field after the 5 days integration period.

9. Page 3495, lines 23-24: Does sigma0 depend on the horizontal resolution?

This is an interesting question. The initial length scale, σ_0, is not expected to depend on the horizontal grid-spacing. However, this can not be tested easily, since the effective length scale σ_e in Eq. (12) depends on the the horizontal grid-spacing.

10. Page 3495, lines 24-36: I do not understand how you reached this conclusion "Therefore, we conclude that for neutral conditions the initial length scale can assumed to be independent of the upstream conditions." Please, clarify.

Thank you for this comment. We intended to state that the value of $\sigma_0 = 1.7\,R_0$ should apply to similar types of turbines. Therefore, it was not appropriate to use "conclude". We propose to delete this sentence on p. 3495 l. 24–26 and to add to on p. 3503 l. 22 the here underlined sentence:

> ...farms are available. We found for the most frequently observed wind speed bin an initial length scale of $\sigma_0 = 1.7\,R_0$ that fitted the turbine measurements the best. We recommend this constant for similar wind turbines. Future wind turbine measurements are needed to confirm this value for other turbine types, such as low induction turbines. This constant ...

11. Page 3497, lines 4-6: You mentioned before that you used different wind speeds at the hub height for validation but here you say that you use 10 m/s. This deserves clarification.

The simulations with a $10\,\mathrm{m/s}$ wind speed were used for the visual analysis related to Fig. 5 (wake recovery compared to measurements), Fig. 7 (analysis of the horizontal wake extension and orientation), and Fig. 8 (qualitative comparison for cross-section of TKE). Additionally, we validate the velocity recovery for all wind speeds (7, 8, 9, 10, and $11\,\mathrm{m/s}$)

in Fig. 6.

This comment is addressed in the introduction of Sect. 5, see response to the second major comment.

12. Same lines as before. Although you use different wind speeds to select sigma0 and validate the parameterization, you focus on the same wind farm and therefore the parameterization is somewhat tuned for this particular site. This hampers the comparison with the WRF-WF parameterization. If you show sensitivities to the values of sigma0 one can have an idea of how important is the specification of this parameter for the results. See also general comment.

This comment is very related to the first major comment, where we have addressed this issue.

13. Would you recommend using the sigma0 herein presented for other wind farms? Or should sigma0 be adjusted for each wind farm?

The initial length scale should be valid for any wind farm. In the future, as more data becomes available, we should be able to verify this hypothesis for different turbine types, such as low induction turbines (with a lower thrust coefficient). See also the answer to comment 10.

14. Page 3499, lines 6-7: The bias in the WRF-WF is not statistically significant. Both the WRF-WF and EWP reproduce the observations within the observational uncertainty.

The reviewer is right that both schemes are within the observational uncertainty, see Fig. 5. On p.3499, l. 6–7, we discuss the bias between the average of the measured wind speed and the modelled wind speed at the 2 met masts, as well as its tendency for different wind speeds.

In the discussion of Fig. 5, we propose to change on p. 3498 l. 4–10:

10

However, the velocity 2 km downstream of the wind farm, at M6, differs between the schemes by 4.7%. This is important, especially if it was used to estimate the power production on a neighbouring wind farm that was located at this distance from the original wind farm. For example, the Rødsand 2 and Nysted offshore wind farm in Southern Denmark are separated by a comparable distance.

to:

At M6, 2 km downstream of the wind farm, the modelled velocity for both schemes is within the uncertainty of the measurements, but it differs between the schemes by 4.7%. The near wake recovery is important, especially if it was used to estimate the power production on a neighbouring wind farm that was located at this distance from the original wind farm. For example, the Rødsand 2 and Nysted offshore wind farm in Southern Denmark are separated by a comparable distance.

Furthermore, we propose to change on p. 3499 l. 1–7:

The WRF-WF scheme shows a positive bias in velocity of up-to $0.5\,\mathrm{m\,s^{-1}}$ at M6. This positive bias, between the WRF-WF scheme and the measurements, becomes larger with increasing wind speed. The bias at M6 is a consequence of the too fast modelled wake recovery from the end of the wind farm to M6. Between M6 and the point at which the free-stream velocity is reached again, the modelled wake recovery is slower than that measured. This overall positive bias implies that the modelled velocity with the WRF-WF scheme is overestimated throughout the whole wake. This overall positive bias implies that the modelled velocity with the WRF-WF scheme is overestimated throughout the whole wake.

to:

The WRF-WF scheme shows a positive difference in velocity of up-to $0.5\,\mathrm{m\,s^{-1}}$ at M6. This difference, between the WRF-WF scheme and the measurements, becomes larger with increasing wind speed. The higher modelled velocity at M6 is a consequence of the more rapid recovery of the modelled wake from the end of the wind farm to M6 compared to that of the measurements. Between M6 and the point at which the free-stream velocity is reached again, the modelled wake recovery is slower than that measured. This overall positive difference suggests that the modelled velocity with the WRF-WF scheme is overestimated throughout the whole wake.

15. Pages 3500 and 3502, Section 5.2. I like this section. It shows large differences between the TKE from the two schemes. This is probably the largest difference between the 2 schemes. If possible, the authors should show figures from the other works mentioned during the discussion to facilitate the comparison of results from both TKE fields.

Thank you for this positive comment and the suggestion to add additional figures. Figure 5

from Wu and Porté-Agel (2013) would perhaps be a useful figure to show. We plan to ask their publisher for permission.

16. Section 5.2: Are you advecting the TKE in the WRF-WF runs? I think by default is turned off in WRF but is better to activate it. Activating the TKE advection may change the shape of the TKE field shown on Fig. 8b.

In WRFV3.3 and WRFV3.4 the TKE was advected per default and we used V3.4 for our simulations. The switch for TKE (bl_mynn_tkeadvect) advection with the MYNN scheme has been introduced only in WRFV3.5. Regarding the TKE advection, we addressed this in the updated Table 2, see comments nr. 7.

17. Conclusions, page 3501, lines 25-26. The bias is not statistically significant. Maybe is better to say that EWP reproduces the wind farm wake within the observational uncertainty.

We agree with the reviewer and propose to change on p. 3504 l. 25–26:

The bias was less than $0.15 \, \mathrm{m\,s^{-1}}$, except for the $7 \, \mathrm{m\,s^{-1}}$ wind speed bin at mast M6, where it was around $0.23 \, \mathrm{m\,s^{-1}}$.

to:

The EWP scheme reproduces the wind farm wake within the observational uncertainty.

18. Page 3506, line 13: Why do you need the power coefficient? It is not mentioned in the description of the EWP parameterization.

The power is not needed for the wind farm wake simulations. It is used, however, to estimate the power production of the wind turbines.

We propose to add on p. 3506 l.13:

. . . in a file. Where the power coefficient is used optionally to estimate the turbine power production. This file name . . .

Appendix A

We use the notation and symbols of Raupach and Shaw (1982), with the exception that the ensemble average is used instead of the time average. The instantaneous velocity, u_i, can be decomposed in a spatial average and a fluctuation around it, $u_i = \langle u_i \rangle + u_i''$ and an ensemble average with a fluctuation, $u_i = \overline{u}_i + u_i'$. Figure 1 illustrates the instantaneous velocity, as well as the spatial and ensemble-averaged velocity in the vicinity of a wake.

We can decompose the total kinetic energy:

$$\frac{1}{2}\langle \overline{u_i^2} \rangle = \frac{1}{2}\langle \overline{u}_i^2 \rangle + \frac{1}{2}\langle \overline{u_i'^2} \rangle \tag{5}$$

$$= \frac{1}{2}\langle \overline{u}_i \rangle^2 + \frac{1}{2}\langle \overline{u}_i''^2 \rangle + \frac{1}{2}\langle \overline{u_i'^2} \rangle. \tag{6}$$

In Eq. (5), we applied an ensemble and spatial averaging to the kinetic energy and we have decomposed the ensemble-averaged kinetic energy in an average and fluctuating part. Here, $\frac{1}{2}\langle \overline{u}_i^2 \rangle$ is the spatial average of the ensemble-averaged kinetic energy and $\frac{1}{2}\langle \overline{u_i'^2} \rangle$ the spatial average of the kinetic energy from random velocity fluctuations.

By decomposing the first term on the r.h.s. of Eq. (5), we obtain Eq. (6). In Eq. (6), we now have three contributions to the total spatial and ensemble-averaged kinetic energy. The first term $\frac{1}{2}\langle \overline{u}_i \rangle^2$ is the kinetic energy of the spatial and ensemble-averaged velocity. The second term $\frac{1}{2}\langle \overline{u}_i''^2 \rangle$ is the spatial-averaged kinetic energy of the heterogeneous part of the mean flow, which is the difference between the ensemble and spatial-averaged kinetic energy. This term arises only in non-homogeneous flow conditions and is also called "dispersive kinetic energy" by Raupach and Shaw (1982).

For each contribution on the r.h.s. of Eq. (6) to the total kinetic energy, a budget equation can be derived. The complete set of equations can for example be found in Raupach and Shaw (1982). We can combine the three components in Eq. (6) to kinetic energy of the mean flow (MKE) and turbulence kinetic energy (TKE). The MKE is not directly resolved by the model. However, the definition of TKE determines how the effect of wind turbines to the TKE is parametrised.

In approach I, one can define MKE $= \frac{1}{2}\langle \overline{u}_i^2 \rangle = \frac{1}{2}\langle \overline{u}_i \rangle^2 + \frac{1}{2}\langle \overline{u}_i''^2 \rangle$ and TKE $= \langle \frac{1}{2}\overline{u_i'^2} \rangle$ (Raupach and Shaw, 1982; Finnigan and Shaw, 2008). Here, the MKE is equal to the spatial average of the ensemble-averaged kinetic energy and it contains all kinetic energy of the organised motion. With this definition only random motion contributes to the TKE. The presence of the drag force gives rise to the source term $\langle \overline{p}_t \rangle = \langle \overline{u' f'} \rangle$, where f' is the fluctuation of the drag force around the ensemble-averaged force. This approach is used in

the EWP scheme and in Sect. 2.2 the additional source term is derived.

In approach II, one could define $\text{MKE} = \frac{1}{2}\langle\,\overline{u}_i\,\rangle^2$ and then the $\text{TKE} = \frac{1}{2}\langle\,\overline{u''_i}^2\,\rangle + \frac{1}{2}\langle\,\overline{u'^2_i}\,\rangle$. In this case, the MKE contains only kinetic energy from the spatial-averaged velocity. Whereas, the TKE contains now also energy from the heterogeneous part of the mean flow additional to the energy from random motion. In this approach, a fluctuation can be decomposed in $u'' = \overline{u}''_i + u'_i$. Therefore, the source term becomes $\langle\,\overline{p}_t\,\rangle = \langle\,\overline{u''\,f''}\,\rangle$, where f'' is the fluctuation of the drag force around the spatial averaged-force. In the WRF-WF, this approach is used (see Sect. 4.1.2).

References

Finnigan, J. J. and Shaw, R. H.: Double-averaging methodology and its application to turbulent flow in and above vegetation canopies, Acta Geophysica, 56, 534-561, doi:10.2478/s11600-008-0034-x, 2008.

Nakanishi, M. and Niino, H.: Development of an improved turbulence closure model for the atmospheric boundary layer, J. Meteorol. Soc. Jpn., 87, 895–912, 2009.

Raupach, M. R. and Shaw, R. H.: Averaging procedures for flow within vegetation canopies, Bound.-Lay. Meteorol., 22, 79–90, doi:10.1007/BF00128057, 1982.

Wu, Y.-T. and Porté-Agel, F.: Simulation of turbulent flow inside and above wind farms: model validation and layout effects, Bound.-Lay. Meteorol., 146, 181–205, 2013.

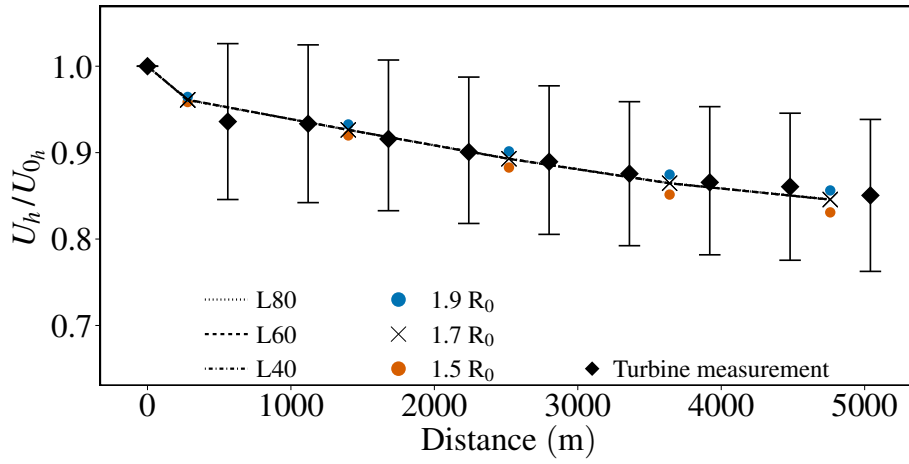Wyngaard, J. C.: Turbulence in the Atmosphere, Cambridge Press, Cambridge, UK, 2010.

Figure 4: Measured and simulated hub-height velocity within the wind farm. The lines show the model simulated velocities averaged over wind direction with an initial length scale $\sigma_0 = 1.7\,R_0$ for the 3 vertical resolutions (L40, L60, and L80). The diamonds represent the measured turbine velocity averaged over each row and the bars indicate their standard deviations. The crosses mark the velocity at the grid-cell centre. The normalised velocity for $\sigma_0 = 1.5\,R_0$ and $\sigma_0 = 1.9\,R_0$ is shown with red and blue dots.
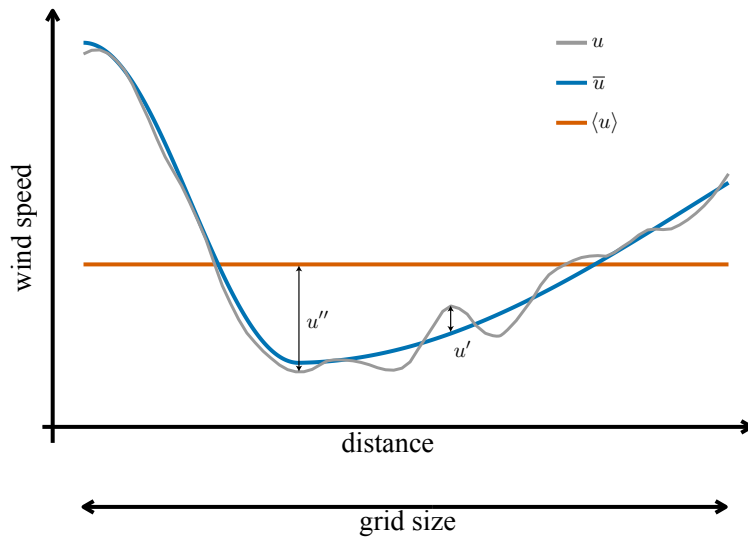
Figure 1: A sketch of the downstream development of a turbine induced velocity reduction. The x-axis indicates the grid-cell size. The grey line represents the instantaneous velocity and the coloured lines the averaged values. The difference between the average and instantaneous velocity defines the turbulence fluctuation at each distance.

We want to thank referee #2 for the valuable comments. We address the comments (in italics bold) on a point by point basis.

1. in Section e 2.2.2, equation 7, the authors assume that the growth rate of the wake is proportional to $x^{1/2}$. This assumption is not correct, as the both numerical and experimental studies of wind turbine wake under the atmospheric conditions show that the wake growth rate has a linear proportionality with x. As a result, the model derivation starts with an assumption that is basically wrong. (It should be noted that this assumption is only valid for the plane wake under laminar inflow condition.)

First, It is important to state here that our focus is on the far wake development as mentioned on p. 3488 l. 13-17 and not on that in the near wake.

Regarding the far wake development, several studies have investigated the downstream wake expansion in the vertical direction, while others examine the downstream decay of the velocity deficit, $\Delta U / U_{ref}$, where ΔU denotes the velocity deficit and U_{ref} the reference wind speed. Iungo and Porté-Agel (2014) study the velocity decay with a LiDAR in atmospheric conditions and Zang et al. (2013) study the velocity deficit decay for a neutral boundary layer in a wind tunnel. Iungo and Porté-Agel (2014) find a median velocity deficit decay of $x^{-0.28}$, whereas the fit between 2 and 16 rotor diameters in Zang et al. (2013) leads to a decay of $x^{-0.81}$. Assuming self-similarity (Tennekes and Lumley, p. 114), this would result in a wake expansion of $x^{0.72}$ for Iungo and Porté-Agel (2014) and $x^{0.19}$ for Zang et al. (2013). Both expansion rates are well below $n = 1$. Stallard et al. (2015) study the wake expansion and the velocity deficit decay behind a turbine in a water tank in a neutral, turbulent boundary layer. They find for the transverse profile a wake expansion close to $x^{1/2}$ and a velocity deficit decay of $x^{-1/2}$. Xie and Archer (2014) investigate the wake expansion with a LES model and compare their results to those from a wind tunnel experiment. They find self-similarity in the velocity deficit profile for low friction velocities. In their Fig. 14b, they could fit a non-linear wake expansion between 0 and 20 rotor diameters to a specific linear function. This example shows that the fitting of the wake expansion is (at these short distance ranges) not very sensitive to the expansion rate.

Given the spread in the estimated wake expansion coefficients n found in the literature, we use the RANS equations (Eq. (5) in the manuscript) to describe the far wake expansion. The resulting wake expansion in Eq. (7) is the same as in classical wake theory for turbulent flows (see for example Schlichting (1968) or Tennekes and Lumley (1972)). In contrast to the fits obtained in the experimental studies, which depend on the specific experimental set-up, the expansion as described in Eq. (7) of the manuscript is a function of stability, and therefore general applicable to different atmospheric conditions.

Finally, the comparison to the measurements shows (our Fig. (4)) that a fairly good

agreement with the measurements is achieved for this approach.

To clarify that the formulation is used for the far wake, we propose to combine on p. 3487 l. 16–17:

> The sub-grid-scale model describes the unresolved turbulence diffusion process that results from turbulence shear production. In this model ...

and p. 3488 l. 15–18:

> The turbine wake is normally divided in a near and far wake, where the far wake begins between one rotor diameter D_0 (Vermeer et al., 2003) and 3 D_0 (Crespo and Hernández, 1996).

to:

> The turbine wake is generally divided into a near and far wake, where the far wake begins between 1 and 3 rotor diameters D_0 (Vermeer et al., 2003; Crespo and Hernández, 1996). The parametrisation describes the unresolved far wake expansion, that is caused by turbulence diffusion. We account for the expansion in the near wake in the initial length scale.

Furthermore, we propose to add the here underlined part of the sentence p. 3488 l. 11–13:

> In Eq. (7), σ_0 denotes the initial length scale, <u>which incorporates the near wake expansion.</u> Equation (7) represents the vertical wake extension, resulting from turbulent diffusion of momentum and it is similar to the solution of Eq. (4.29) in Wyngaard (2010) for the dispersion of plumes. ...

In the discussion section, we would motivate our choice and discuss further investigations. We would add the here underlined paragraph on p. 3502 l. 18:

> ... remain unresolved.
> <u>In the proposed parametrisation, we use the classical wake theory (Tennekes and Lumley, 1972) to describe the sub-grid-scale wake expansion. Compared to empirical fits from for example Zang et al. (2013) and Xie and Archer (2014), it offers the advantage that the wake is described as a function of stability. In this study, we have validated the approach for different wind speeds. Its performance for atmospheric stability, which requires information of the profiles, will be investigated in future.</u>

2. The authors mention that the definition of TKE in their model is different from the one in Fitch et al. (2012). If this is the case (the definition of TKE is different in different schemes), how the authors compare their results with the ones obtained from WRF-WF scheme?

The TKE definition in the EWP and WRF-WF scheme differ, this affects only the parametri-

sation of the additional source term P_t. The governing equation is exactly the same (except for the source term P_t). We recall that fluctuations remain unresolved and the TKE is completely parametrised as a function of mean quantities. From a mathematical point of view the two quantities are therefore comparable.

In Sect. 5, we propose to change on p. 3497 l. 8–11:

In a qualitative validation, we examine the simulated wind farm wake characteristics, as well as the vertical profile of the wake deficits, using results from LES simulations and wind tunnel experiments as a reference.

to:

In a qualitative validation, we examine the velocity reduction behind the wind farm and the vertical profile of the velocity deficit. Furthermore, we discuss the vertical structure of the modelled TKE field from the discretized Eq. (3), where the additional source term $\langle \overline{p_t} \rangle$ has been parametrised in the WRF-WF scheme and neglected in the EWP scheme. We use results from independent LES simulations and wind tunnel experiments as a reference.

Furthermore, we propose to update the final paragraph of the discussion on p. 3504 l. 2–9:

... of large wind farms. For the WRF-WF and EWP scheme, the PBL scheme adjusts the TKE production through the changed vertical shear in horizontal velocity. The term that represents the local turbine-induced turbulence is neglected in the EWP approach, whereas it is parametrised as an additional source term in the WRF-WF scheme. The total TKE is more than 3 times larger in the WRF-WF scheme than in the EWP scheme. Future measurement campaigns around large wind farms under suitable atmospheric conditions can help to settle this issue.

to:

... of large wind farms. Both wind farm schemes use a PBL scheme that parametrises the TKE equation in terms of grid-cell averaged variables. Therefore, in the wake of the wind turbines TKE is generated by the increased vertical shear in horizontal velocity. Then, the different definition of the unresolved velocity fluctuation in the WRF-WF and EWP scheme leads to a different source term $\langle \overline{p_t} \rangle$ that is the direct consequence of the presence of a drag force. In the EWP scheme, a velocity fluctuation is defined around the ensemble-averaged velocity. With this definition $\langle \overline{p_t} \rangle$ is small and can be neglected. Instead, in the WRF-WF scheme velocity fluctuations are defined around the grid-cell averaged velocity and a parametrisation of $\langle \overline{p_t} \rangle$ is added to the model TKE equation. The simulations have shown that in the WRF-WF scheme $\langle \overline{p_t} \rangle$ dominates over the shear production and that its total TKE is several times larger than that in the EWP scheme. However, it is unclear how well the actual grid-cell averaged shear production is approximated by the shear production calculated with the PBL scheme in WRF, on which the EWP scheme relies.

Therefore, future measurement campaigns of the actual structure and intensity of the TKE field within and around wind farms under suitable atmospheric conditions can help to settle this issue.

3. In comparison with the field data, the authors only validate their model only for the mean velocity, without any comments for the prediction of the added TKE. The author should comment on this issue that which model (EWP or WRF-WF) could provide better estimation for the added TKE inside a wind farm, since the TKE in the wake is responsible for the wake recovery and has significant effects on the power output from downwind turbines.

The data-set for the Horns Rev I wind farm, contained 10 min averaged measurements and no quantitative validation of the TKE field is possible. Therefore, we compare the structure of the TKE field against that from LES simulations only qualitatively. Furthermore, we compare the internal boundary layer growth, which is related to the additional turbulence. In the discussion, we mentioned on p. 3504 l. 7–9 that future campaigns are needed to measure the structure of the TKE field.

For clarity, we propose to repeat the use of 10-min averaged wind speeds on p. 3492 l. 10:

... The 10-min averaged data from the two ...

and on p. 3493 l. 1:

... we select the 10-min averaged wind speeds ...

4. In section 2.2, the authors mention that "The expression for Pt can be found by multiplying the NavierStokes equations with the velocity fluctuation and then applying Reynolds averaging" However, in equation 4, a negative sign is missing (F_{Di} has a negative sign). As a result, the equation 4 is always negative and cannot predict the augmentation of turbulence due to the presence of the turbines.

We want to thank the reviewer for pointing this out. Indeed, the term in Eq. (4) should contain a minus sign. This has no implications on the EWP scheme and the results, since the term has been neglected in the parametrisation anyway. The source term we described on p. 3487 l.1–7 would require the simulation of the full blade structure and cannot be described by the drag force in Eq. (1). On the other hand, as pointed out by the reviewer, Eq. (4) represents a sink of TKE due to the momentum sink. This TKE term contributes to the electrical power production and mechanical losses in structures and transmission. For the Vestas V80 turbine, the absolute value of this additional term is around 30 times smaller than the additional term P_t in Eq. (16) from the WRF-WF

4

parametrisation and can, therefore, be neglected. For example, for a wind speed of $10\,\mathrm{m\,s^{-1}}$ we have $c_t = 0.79$, $c_p = 0.43$, and $\langle \overline{u'_i\,u'_i} \rangle = 0.7\,\mathrm{m^2\,s^{-2}}$ at hub-height. This gives for $\langle \overline{p_{t,\mathrm{WRF\text{-}WF}}} \rangle / \langle \overline{p_t} \rangle = 0.5\,(c_t - c_p)\,u^2/(c_t\,\langle \overline{u'_i\,u'_i} \rangle) = 32$.

In the manuscript, we propose to

1) add the minus sign to the second and third term in Eq. (4).

2) change on p. 3487 l. 1–7:

> This additional turbulence occurs directly behind the turbine blades. Its turbulence length scale ℓ is expected to scale with the blade's cord length, which is on the order of a few metres and it is therefore much smaller than that of the atmospheric flow. The smaller length scale implies a significant higher dissipation rate $\epsilon \propto (1/\ell)\overline{u_i u_i}^{3/2}$. Therefore, we assume the source term in Eq. (4) to dissipate within a mesoscale model grid-cell and neglect P_t of Eq. (4) on the grid-cell average.

to:

> This term represents a sink of TKE due to the extraction of momentum. The magnitude of this term is much smaller than the additional source term in the WRF-WF scheme (see Sect. 4.1.2). Therefore, the additional term $\langle \overline{p_t} \rangle$ in the EWP approach is neglected.

3) substitute on p. 3496 l. 16–18:

> The TKE source term from the WRF-WF scheme in Eq. (16) is much larger than the source term in Eq. (4), which comes from the different definition of TKE in the two schemes.

with:

> For the considered wind speeds the absolute value of $\langle \overline{p_{t,\mathrm{WRF\text{-}WF}}} \rangle$ is around 30 times larger than $\langle \overline{p_t} \rangle$ defined in Eq. (4), which comes from the different definitions of TKE in the two schemes. For example, for $10\,\mathrm{m\,s^{-1}}$ with $c_t = 0.79$, $c_p = 0.43$, and $\langle \overline{u'_i\,u'_i} \rangle = 0.7\,\mathrm{m^2\,s^{-2}}$ at hub-height, the ratio between $\langle \overline{p_{t,\mathrm{WRF\text{-}WF}}} \rangle$ and $\langle \overline{p_t} \rangle$ as it has been defined in Eq. (4) is 32.

It should be noted that, inside a grid cell, the heterogeneity of the flow is not resolved. It means that we cannot resolve the velocity inside the gird as shown in Fig.1a, and what we have is the averaged one over the grid cell (Fig. 1b). Therefore, all the heterogeneity inside the grid cell must be taken into account in the parametrization in order to estimate the added TKE by the turbines. Otherwise, as shown in Eq. (4) (with a negative sign), this formulation only predicts the reduction of turbulence inside the farm, which is not correct.

The definition of the velocity perturbation and the description of the averaging is an im-

portant part of the manuscript and we propose to update Sect. 2 to make it as clear as possible. The proposed text can be found at the end of the document. First, we address the individual reviewer's statements below.

It should be noted that, inside a grid cell, the heterogeneity of the flow is not resolved. It means that we cannot resolve the velocity inside the gird as shown in Fig.1a, and what we have is the averaged one over the grid cell (Fig. 1b).

We agree with the reviewer that within the grid-cell the heterogeneity of the flow remains unresolved and that only the grid-cell averaged velocity is resolved.
In Fig. 1, we intended to illustrate the difference in the velocity fluctuation that occurs from the different definition of the average velocity. In the revised text, the illustrative purpose for the definition of the velocity perturbation will be stated more clearly.

Therefore, all the heterogeneity inside the grid cell must be taken into account in the parametrization in order to estimate the added TKE by the turbines.

The main reason for including TKE is that it can be used to parametrise fluxes. These are turbulent fluxes driven by random motion, but not all heterogeneity is random. Therefore, only the random part of the fluctuation should be considered.

Otherwise, as shown in Eq (4) (with a negative sign), this formulation only predicts the reduction of turbulence inside the farm, which is not correct.

It is important to consider the parametrisation in conjunction with the WRF model and not as a standalone model.
In the EWP scheme the additional term P_t in Eq. (4) has been neglected (independent of it being a source or sink term), since this term acts only locally at the turbine and is on a spatial average very small compared to the other terms in the TKE equation (see previous comment). However, the EWP approach relies on the turbulence shear production (P_s) from the PBL scheme. Therefore, the parametrisation embedded in the WRF model predicts, as a consequence of the changed velocity shear, an increased TKE above and a decreased TKE below hub-height compared to the background flow and does not predict a reduction of turbulence inside the wind farm (Fig. 8) as has been stated by the reviewer.

Regarding the averaging, we have proposed several changes (see first specific comment of referee #1) and prepared an appendix that can also be found in the reply to referee #1.

References

Crespo, A. and Hernández, J.: Turbulence characteristics in wind-turbine wakes, J. Wind. Eng. Ind. Aerod., 61, 71–85, 1996.

Iungo, G.-V. and Porté-Agel, F.: Volumetric scans of wind turbine wakes performed with three simultaneous wind LiDARs under different atmospheric stability regimes, Journal of Physics: Conference Series 524, 2014. doi:doi:10.1088/1742-6596/524/1/012164

Finnigan, J. J. and Shaw, R. H.: Double-averaging methodology and its application to turbulent flow in and above vegetation canopies, Acta Geophysica, 56, 534-561, doi:10.2478/s11600-008-0034-x, 2008.

Nakanishi, M. and Niino, H.: Development of an improved turbulence closure model for the atmospheric boundary layer, J. Meteorol. Soc. Jpn., 87, 895–912, 2009.

Raupach, M. R. and Shaw, R. H.: Averaging procedures for flow within vegetation canopies, Bound.-Lay. Meteorol., 22, 79–90, doi:10.1007/BF00128057, 1982.

Schlichting, H: Boundary layer Theory, McGraw-Hill Book Company, Sixth edition, 1968.

Stallard, T., Feng, T., and Stans, P.K.: Experimental study of the mean wake of a tidal stream rotor in a shallow turbulent flow, Journal of Fluids and Structures, 54, 235246, 2015, doi:doi:10.1016/j.jfluidstructs.2014.10.017.

Tennekes, H. and Lumley, J. L.: A First Course in Turbulence, The MIT Pess, Boulder, USA, 1972.

Vermeer, L. J., Søensen, J. N., and Crespo, A.: Wind turbine wake aerodynamics, Prog. Aerosp. Sci., 39, 467–510, 2003.

Wyngaard, J. C.: Turbulence in the Atmosphere, Cambridge Press, Cambridge, UK, 2010.

Xie, S., Archer, C.: Self-similarity and turbulence characteristics of wind turbine wakes via large-eddy simulation, Wind Energy (2014) doi:DOI: 10.1002/we.1792

Zhang, W., Markfort, C. D., and Porté-Agel, F.: Wind-Turbine Wakes in a Convective Boundary Layer: A Wind-Tunnel Study, Bound.-Lay. Meteorol. 146, 161179, 2013 doi:DOI 10.1007/s10546-012-9751-4.

We would like to thank referee #3 for the valuable comments. We address the comments (in italics bold) on a point by point basis.

General Comments
The authors present a new parameterization of wind farms for mesoscale models, in particular for WRF. The explicit model is well described in the formulation as far as I understand, although I admit I havent reproduced the equations myself. There is however little justification as to how the freestream is selected or the individual source terms of the turbines aggregated to the grid-cell values. Adopting a common cell velocity U0 and adding individual thrust forces together to form the grid-cell overall thrust is an ad hoc solution that seems appropriate as first approximation.

As a first approximation, we use the available model information (spatial-averaged variables) to calculate the single turbine thrust forces (similar as in the WRF-WF scheme). As shown in Abkar and Porté-Agel (2015), this approximation holds for wind directions in which the turbines are aligned. However, for more complicated configurations, the local free-stream velocity is expected to deviate from the grid-cell velocity. In Badger et al. (2013), we introduce an offline coupling method, where the total thrust on the l.h.s. of Eq. (8) is determined as a function of wind speed and wind direction (and optionally stability) from high resolution models. This method has been implemented in the WRF model and in the future we would like to add this as an option. We discuss this issue on p. 3502 l. 15 to p. 3503 l. 4.

Then σ_0 is used to calibrate the wake model to the Horns Rev results. The doubt resides on whether this calibration holds for completely different layouts. For example, a layout occupying the same space that Horns Rev and with the same type and number of turbines but very different distribution would produce the same wind farm wake following this methodology. I agree with the authors that further research would try to account for the specific layout of the wind farm to generate grid-cell values without calibration.

The reviewer is right that current wind farm parametrisations do not account for the individual turbine positions within the grid-cell. The method described in Badger et al. (2013) accounts for the turbine positions, since it applies the drag from the micro-scale model. As soon as data from different wind farms (with wind farm wake measurements) becomes available, we will compare the presented approach with that of Badger et al. (2013).

There is very little research so far on mesoscale-simulated wakes so I think

that the paper is worth for publishing and I look forward to further efforts with this model in the future. The following remarks shall be considered to provide further justification to the evaluation methodology of the paper.

Thank you for this positive comment. The reviewer is right that little research has been done in the mesoscale modelling of wakes. In our opinion mesoscale models cannot only be a useful tool to study the impact of wind farms to the local climate, but it could also be used to study wind farm interaction, which is an important issue with the increasing wind farm density in the North-Sea.

Specific Comments

Page.3482 Line.23: I would remove "in Northern Europe and China" to make the statement general to coastal areas

On p. 3482 l.23 we would remove "in Northern Europe and China".

P3491, L.7: It is not so clear why the cell-velocity is representative of a common upstream velocity for the whole wind farm.

Actually, the grid-velocity is only used as a upstream wind speed for the local turbines within that cell.

We propose to rephrase the sentence on p. 3491 l. 7–8:

> We use the grid-cell averaged velocity as the upstream velocity U_0 to the wind turbine.

with:

> We use the grid-cell averaged velocity as the upstream velocity U_0 for all turbines within the same grid-cell.

P.3491, L.13: add Section number.

Thank you. We would replace p. 3491 l. 12–13:

> A practical description of how to use the EWP scheme in the WRF model is given in Sect. .

with:

> A practical description of how to use the EWP scheme in the WRF model is given in the section "Code availability" at the end of the paper.

2

P.3493, L.21: Can you provide a reference for the roughness length or justify why the value of 2e-4 m has been adopted?

We have used this value from the WMO standard roughness length over water.

We propose to change on p. 3493 l. 20:

> The surface roughness was constant in time and set to $z_0 = 2 \times 10^{-4}$ m for the entire domain.

to:

> The domain is fully contained over water and it had a constant roughness length of z_0 = 2×10^{-4} m in time, which follows the WMO standards.

P.3494, L.4: Why slightly-stable atmosphere when the validation data is considered neutral?

The slightly stable atmosphere initialised in WRF converged to a completely neutral PBL, since the surface heat flux was set to zero (see 7th specific comment of the 1st reviewer).

P.3494, L.7: What is the lapse rate of the inversion layer? Probably not a big influence on the results but should be documented since it is an input in the idealized simulations.

The lapse rate of the potential temperature is around $6.0\,\mathrm{K/km}$ within the inversion layer.

We propose to change on p. 3494 l. 5–7:

> After a four day integration period, the wind converged in the whole domain to a logarithmic neutral profile within a 650 m deep boundary layer and remained independent of height above the inversion layer.

to:

> After a four day integration period, the wind converged in the whole domain to a logarithmic neutral profile within a 650 m deep boundary layer capped by inversion layer with a potential temperature gradient of around $6\,\mathrm{K/km}$. Above the inversion layer the velocity became independent of height.

P.3494, L.16: Was the averaging of the 9 wind direction runs done using a uniform directional distribution or considering the weighted-average following the actual distribution observed in the 30deg sector width? The result can be quite different depending on the averaging procedure

3

The averaging was done with the uniform direction distribution.

We propose to change on p. 3494 l. 16:

> For the validation against the mast measurements, we averaged the model wind speeds over the 9 wind directions.

to:

> For the validation against the mast measurements, we averaged the model wind speeds over the 9 wind directions with a uniform direction distribution.

P.3494, L.24: It is not clear how the length scale is determined based on the wind speed. Can you clarify this point? Maybe it is just enough to say that the initial length scale should be in first approximation equal to the rotor area. Then you introduce the idea of using the scaling factor to calibrate the model results to the observational data.

Thank you for this comment. The initial length scale is supposed to scale with the rotor area, but it includes the near wake expansion.

We propose to rephrase on p. 3494 l. 24–26:

> To a first approximation the initial length scale is defined to be independent of the upstream conditions and it is therefore the same for all turbines.

to:

> To a first approximation, the initial length scale is defined to be independent of the upstream conditions and it is therefore the same for all turbines. The initial length scale is assumed to scale with the rotor radius and accounts for the near wake expansion.

Figure 9: It would be useful to show the undisturbed upstream velocity profile from both the WRF-WF and EWP models to show that they are actually the same or very similar.

In the attached figure, we show the upstream velocity profiles from the EWP and WRF-WF scheme from the same grid-cell as has been used for Fig. 9. The two curves are indistinguishable from each other. In case the reviewer or editor would like to have this figure included in the manuscript, we would add it. Otherwise, we would mention in the text that the up-stream profiles very visually the same.

We propose to add the here underlined text on p. 3501 l. 18:

> . . . farm simulation. <u>The free-stream velocities are visually indistinguishable between the EWP and WRF-WF simulation.</u> We choose . . .

References

Abkar, M. and Porté-Agel, F.: A new wind-farm parameterization for large-scale atmospheric models, J. Renewable and Sustainable Energy, 7, 013121, doi:10.1063/1.4907600, 2015.

Badger, J., Volker, P. J. H., Prospathospoulos, J., Sieros, G., Ott, S., Rethore, P.-E., Hahmann, A. N., and Hasager, C. B.: Wake modelling combining mesoscale and microscale modelsm, in: Proceedings of ICOWES, Technical University of Denmark, 17–19 June 2013, Lyngby, p. 182–193, available at: `http://indico.conferences.dtu.dk/getFile.py/access?resId=0&materialId=paper&confId=126`, 2013.
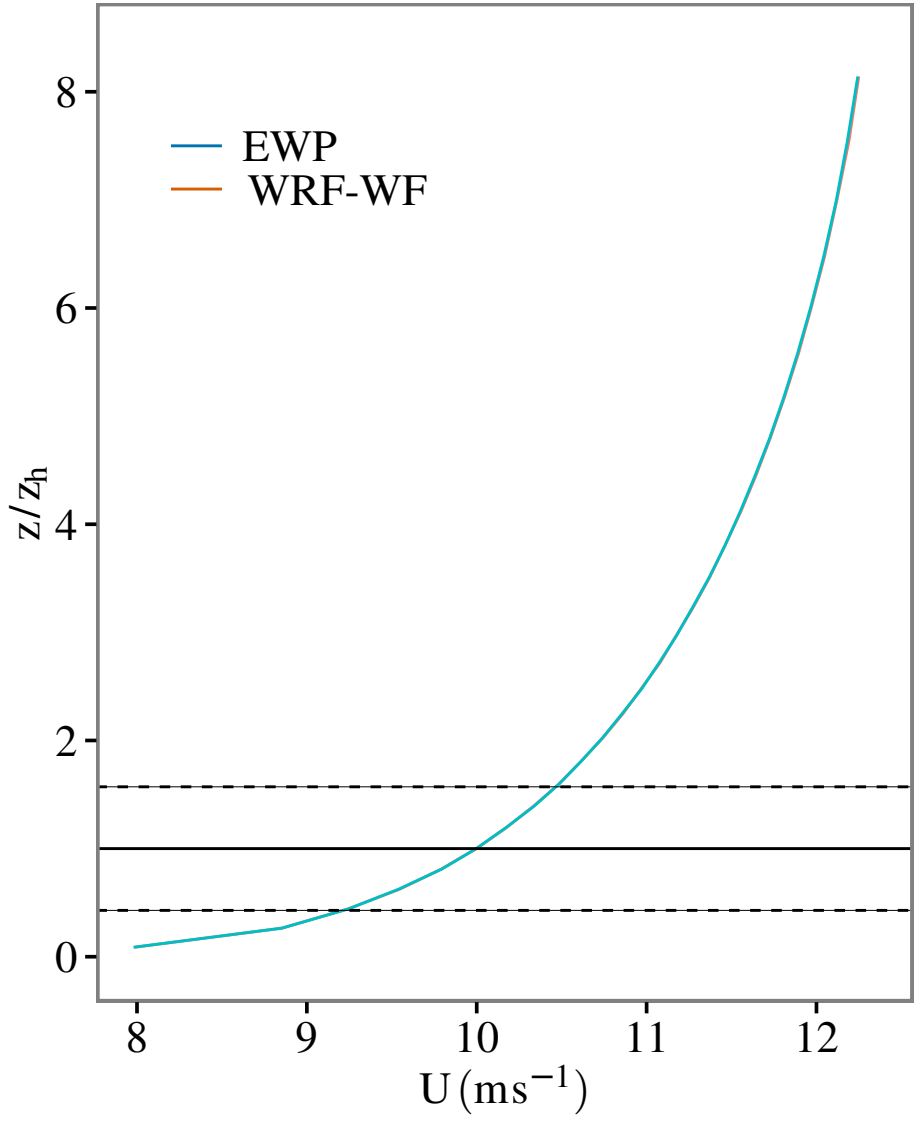
Figure 1: Upstream velocity profile from the EWP and WRF-WF.

We are thankful for the comments of Dr. Anna Fitch. Below we address all comments (italic and bold) and specify the position of the proposed updated text.

1. Page 3482 lines 21-22: citations regarding high resolution simulations of the impact of wind turbines on boundary layer flow are missing, including Calaf et al. (2010), Porté-Agel et al. (2011), Lu and Porte-Agel (2011), Fitch et al. (2012, 2013a). Further observational studies include Smith et al. (2013) and Rajewski et al. (2013). Also of relevance are wind tunnel studies e.g. Zhang et al. (2013).

Thank you for the suggested literature. We would add Calaf et al. 2010, Lu and Porté-Agel (2011), and Fitch at. al (2013)a to the literature. However, the study of Porté-Agel et al. (2011) is similar to that of Wu and Porté-Agel (2013), which we already use as a reference. Smith et al. (2013) and Zhang et al. (2013), study mostly the changed heat-fluxes due to wind farms, whereas we have simulated neutral conditions without heat-fluxes in our simulations.

2. Page 3483 lines 27-28: here you might like to mention Fitch et al. (2013b) who compare the roughness and elevated drag approaches.

Thank you for suggesting this interesting work. We would add this reference.

3. Page 3484 lines 12-13: the name WRF-WF has not been used in prior work, this should be re-worded e.g. "here denoted as WRF-WF". Similarly with page 3496 lines 1-3. Also, Fitch et al. (2012) describe the parameterization and model formulation whereas Jimenez et al. (2014) compare the parameterization with observations.

Following the comment from Anna Fitch, we would update on p. 3484 l. 12–13:

> ...The WRF model already includes a wind farm parametrisation option, WRF-WF (Fitch et al., 2012; Jiménez et al., 2014) ...

to:

> ...The WRF model already includes a wind farm parametrisation option (Fitch et al., 2012; Jiménez et al., 2014), which we will denote as WRF-WF ...

4. Page 3496 line 2: it was introduced in WRF version 3.3.

Thank you for bringing this to our attention. This would be corrected in the manuscript.

5. Page 3496 lines 20-23: Fitch et al. (2012, 2013a,b) use both turbine thrust

and power coefficients from a real wind turbine, and it is stated in the WRF model instructions that the idealized data included in the model should be replaced with actual coefficients for the particular turbine of interest (obtained from the turbine manufacturer). The formulation of the parameterization is not based on an empirical relationship. The reason real data was not included in the model was due to legal considerations with turbine manufacturers who do not release this data into the public domain. Idealized thrust and power coefficients are included in the model instead as an example, with the caveat that they are for testing purposes only, not for scientific work. A note regarding this issue in more detail will appear in the journal Wind Energy.

Thank you for this comment. We, however, did not intend to state that the formulation of the parametrisation is based on an empirical relationship. On p. 3496, we described that in WRFV3.4 the thrust coefficient was determined in the WRF-WF module from the power coefficient. Later, in WRFV3.6 both coefficients could be provided via an ASCII file per default. To accommodate also the second major comment of the first reviewer, we would update the final paragraph on p. 3496 l. 19–24 from:

> In WRFV3.4, the WRF-WF parametrisation the power coefficient has been obtained from the power curve information. The thrust coefficient was then determined by an empirical relationship with the power coefficient. Jiménez et al. (2014) improved the performance of the WRF-WF scheme in a comparison against turbine measurements of the Horns Rev I wind farm by using both a turbine thrust and power coefficient. This approach is used in the experiments performed in Sect. 5.

to:

> In Sect. 5, we use the up-dated WRF-WF parametrisation from WRFV3.6, which has no free parameters. The power and thrust coefficients come from the Vestas V80 turbine.

6. Page 3502 lines 10-13: wind acceleration at low levels has been observed by Rajewski et al. (2013).

Thank you for the link to this interesting work. This study, shows velocity profiles in front of and behind a wind turbine for one night in Mid-Summer in the Great Plains. The simulation of this particular case study, would require detailed information about the atmospheric conditions during that night. Therefore, we would prefer to compare the wake profiles from our study (neutral conditions) to profiles that were obtained under similar conditions.

References:

2

Barrie, D. B. and Kirk-Davidoff, D. B. Weather response to a large wind turbine array. Atmos. Chem. Phys., 10:769775, 2010.

Calaf, M., C. Meneveau, and J. Meyers, 2010: Large eddy simulation study of fully developed wind-turbine array boundary layers. Phys. Fluids, 22, 015110, doi:10.1063/1.3291077

Fitch, A. C., J. K. Lundquist, and J. B. Olson, 2013a: Mesoscale influences of wind farms throughout a diurnal cycle. Mon. Wea. Rev., 141, 21732198.

Fitch, A. C., J. B. Olson, and J. K. Lundquist, 2013b: Parameterization of Wind Farms in Climate Models. J. Climate, 26, 64396458. doi: http://dx.doi.org/10.1175/JCLI-D-12-00376.1.

Jiménez, P. A., Navarro, J., Palomares, A. M., and Dudhia, J.: Mesoscale modeling of offshore wind turbine wakes at the wind farm resolving scale: a composite-based analysis with the Weather Research and Forecasting model over Horns Rev, Wind Energy, 18, 559566, 2014.

Kirk-Davidoff, D. B. and Keith, D. W. On the climate impact of surface roughness anomalies. J. Atmos. Sci., 65:2215-2234, 2008.

Lu, H., and F. Porté-Agel, 2011: Large-eddy simulation of a very large wind farm in a stable atmospheric boundary layer. Phys. Fluids, 23, 065101, doi:10.1063/1.3589857.

Porté-Agel, F., Y.-T. Wu, H. Lu, and R. J. Conzemius, 2011: Large-eddy simulation of atmospheric boundary layer flow through wind turbines and wind farms. J. Wind Eng. Ind. Aerodyn., 99, 154168, doi:10.1016/j.jweia.2011.01.011.

Rajewski, D., and Coauthors, 2013: Crop Wind Energy Experiment (CWEX): Observations of surface-layer, boundary layer, and mesoscale interactions with a wind farm. Bull. Amer. Meteor. Soc., 94, 655672.

Smith, C. M., R. J. Barthelmie, and S. C. Pryor, 2013: In situ observations of the influence of a large onshore wind farm on near-surface temperature, turbulence intensity and wind speed profiles. Environ. Res. Lett, 8, 034006.

Wang, C. and Prinn, R. G. Potential climatic impacts and reliability of very large-scale wind farms. Atmos. Chem. Phys., 10, 2053:2061, 2010.

Wu, Y.-T. and Porté-Agel, F.: Simulation of turbulent flow inside and above wind farms: model validation and layout effects, Bound.-Lay. Meteorol., 146, 181–205, 2013.

Zhang, W., C. D. Markfort, and F. Port-Agel, 2013: Experimental study of the impact of large-scale wind farms on land-atmosphere exchanges. Environ. Res. Lett, 8, 015002.

We would like to thank the topical editor for his dedicated time and his comments. We address the comments (in italics bold) on a point by point basis.

I appreciate your thorough replies to all reviewer comments and your changes to the text (even though you included only some of your proposed changes in the revised manuscript). Before accepting the manuscript, several wording issues must be improved. In particular the newly added text parts contain sloppy formulations. In the following the pages and line numbers refer to the manuscript version with the highlighted changes.

Below the specific comments of the topical-editor can be found (italic). Our reply is in times. Additionally, the position in the difference document that is part of the author's response is indicated.

p14,l24: "lower": do you mean the "near ground" atmospheric stability? Your formulation is confusing.
We intended indeed the stability near to the ground. The updated text can be found on p. 15 l. 8.

p15, l13: Better write "The total domain is located over water and we prescribe a constant ...". "in time" can be deleted.
We agree with the topical-editor and have updated this sentence on p. 15 l. 25.

p15, l20: to investigate THE
As has been proposed by the topical-editor, we have changed "a" to "the" (p. 16 l. 6).

p16, l7: Is this what you wanted to say: We ended up with the desired magnitude of the geostrophic wind by conducting several experiments with different initialisation.
This is what we wanted to say. The updated text is on p. 16 l. 22.

p17,l26: According to Fitch it should be V3.3. Generally my impression is, that in your replies you proposed text changes, which you have not yet included in the revised manuscript. And others which you have included. This makes the evaluation harder. So for the next iteration please include all of your proposed corrections.
The topical-editor is right, the version number from which the WRF-WF has been included in the WRF code was not updated. It has this time be updated on p. 18 l. 12.

p19,l13: length scale of EWP → length scale used in EWP?
This update can be found on p. 20 l. 2.

p20,l7: whereas for the WRF-WF.... you may re-formulate this part of the sentence or split apart from the first part.
We have tried to improve the readability of the sentence by splitting it in two sentences (p. 20 l. 16).

p25, l5: "wake PROPERTIES are" better?
If the topical-editor agrees, we would write "expansion" instead of "properties" (p. 25 l. 21).

p25, l7: "Its performance FOR (??) atmospheric stability, which requires information of the profiles, will be investigated in future." Better describe what you mean.
The updated text can be found on p. 25 l. 23.

p25,l13: Future implementations may account for ...
This update can be found on p. 26 l. 3.

p25,l29: besides a ... analyses: delete "a" or write analysis.
Thank you for pointing this out. The corrected text can be found on p. 26 l. 21.

p26,l3: with different vertical resolutions
We have updated the text and it can be found on p. 26 l. 23.

p26,l11: why confirm? wouldn't be "determine" more appropriate?
The topical-editor is right. We have substituted "confirm" with "determine" on p. 27 l. 2.

p28,l6: agree
This has been updated on p. 28 l. 24.

A.) I think it would be fair to mention in the abstract, that only a neutral profile was used in the simulations.
We agree with the topical-editor. We propose to write: The EWP scheme is validated "for a neutral atmospheric boundary" layer against filtered in situ measurements from two meteorological masts situated a few kilometres away from the Danish offshore wind farm Horns Rev I. (p. 2 l. 6).

B.) It is not necessary to add the figure you attached to the response to reviewer #3.
Thank you, we will not add the figure.

C.) Rev #1, 9: Please add to the text the caveat that sigma depends on reso-

2

lution.

We have mentioned on p. 12 l. 3: "Here σ_e is the effective length scale that is related to the model grid-size". Since we have an expression of σ_e, we do not think it is a caveat as such.

D.) p28,l3: If I understood your work correctly, then i am not happy with the word "observational uncertainty". Does it refer to Fig. 5? This does show the observed variability (plus probably including obs. uncertainty). The quite large spread may be reduced, if one could split the observations in several subsets that have distinctly different mean values. Would be atmospheric stability such a candidate? The same thoughts apply to Fig. 4? Could you introduce a variable, which groups the observations in distinct subsets and then implies a sigma-definition that depends on this variable?

We want to thank the topical-editor for this suggestion. One problem of additional splitting is the size of the data-set. Filtering on stability would reduce the data-set such that it becomes too small to allow for statistics (e.g. 140 measurement are under neutral conditions). We agree, however with the topical-editor that the expression "observational uncertainty" is not completely appropriate. We propose to substitute it with "standard deviation of the measurements" (p. 28 l. 20).

E.) Concerning your proposition to include Fig. 5 of Wu & Porté-Agel: The simplest would be to ask the authors for a slightly modified version of the published figure. As far as I know this avoids copyright issues. If you think including the figure makes the paper stronger, then go ahead. Still ask the editorial office for legal issues.

Regarding the figure, we have contacted the publisher to avoid any legal issues.

The Explicit Wake Parametrisation V1.0: a wind farm parametrisation in the mesoscale model WRF

P. J. H. Volker, J. Badger, A. N. Hahmann, and S. Ott

Wind Energy Department, Technical University of Denmark, Risø Campus, Roskilde, Denmark

Correspondence to: P. J. H. Volker (pvol@dtu.dk)

Abstract

We describe the theoretical basis, implementation and validation of a new parametrisation that accounts for the effect of large offshore wind farms on the atmosphere and can be used in mesoscale and large-scale atmospheric models. This new parametrisation, referred to as the Explicit Wake Parametrisation (EWP), uses classical wake theory to describe the unresolved wake expansion. The EWP scheme is validated for a neutral atmospheric boundary layer against filtered in situ measurements from two meteorological masts situated a few kilometres away from the Danish offshore wind farm Horns Rev I. The simulated velocity deficit in the wake of the wind farm compares well to that observed in the measurements and the velocity profile is qualitatively similar to that simulated with large eddy simulation models and from wind tunnel studies. At the same time, the validation process highlights the challenges in verifying such models with real observations.

1   Introduction

Wind turbines capture the kinetic energy of the wind with their turning blades, which transfer the energy to a transmission system that drives an electric generator. In this process the flow in front and behind a wind turbine is decelerated by the forces acting on the rotating blades. In large wind farms, the interaction of the flow and the wind turbines is further complicated by the interaction of the wake of one wind turbine with neighbouring turbines. Besides the changed velocity field around the turbines, there is also evidence that wind turbines affect planetary boundary layer (PBL) processes due to the changed turbulence (Baidya Roy et al. (2004), Calaf et al., 2010 ; Baidya Roy and Traiteur (2010); Barrie and Kirk-Davidoff (2010); Wang and Prinn (2010); Lu and Porté-Agel, 2011 ; Hasager et al. (2013), , and Fitch et al., 2013a).

Coastal regions ~~in Northern Europe and China~~ are expected to become major areas for wind energy production, since winds there are generally strong, steady, and less turbulent. To obtain an optimal yield, which is among others a function of power production, electrical

cabling, and installation costs, it is often convenient to group wind farms together. Examples are the Danish Rødsand 2 and Nysted or the Belgian Belwind, Northwind, and Thornton wind farms, in which the wind farm separation is only a few kilometres. In planning new wind farms near existing ones it is important to estimate the velocity perturbation from the nearby farm as accurately as possible, because the power production is highly sensitive to the wind speed. Velocity deficits behind wind farms can be considerable. Christiansen and Hasager (2005), for example, found for near neutral atmospheric stability, velocity deficits of 2 % up-to 20 km downstream of the Horns Rev I (25 km^2) wind farm. The accurate measurement of wakes from nearby farms becomes even more important in light of the fact that as of 2015 large offshore wind farms cover areas of up-to 100 km^2. Mesoscale models are suitable tools to estimate wind energy resources in these sea areas (Hahmann et al., 2014). However, the collective effect of the wind turbines to the flow needs to be included in these models and because these occur at scales smaller than the model's grid-size and remain unresolved, the effects have to be parametrised.

The parametrisation of the effect of wind turbines largely depends on the model and its mesh size. For instance Large Eddy Simulation (LES) models, while resolving the local flow around wind turbines, need to parametrise the local drag forces on the turbine blade (Porté-Agel et al., 2011; Wu and Porté-Agel, 2013). The grid spacing of mesoscale models, on the other hand, is on the order of kilometres and tens of metres in the horizontal and vertical direction, respectively. This means that the profile of the turbine-induced velocity deficit can be captured to some extent in the vertical direction. However, the downstream development of the velocity remains completely unresolved for scales smaller than the grid size. The major challenge in the parametrisation is to account for the unresolved relevant processes in agreement with the flow equations of the model. In recent years, steady progress has been made in the parametrisation of the effect of wind farms in global and mesoscale models: from the representation of wind farms by an increased roughness length in Keith et al. (2004) and Frandsen et al. (2009), up-to the more advanced drag approaches in Adams and Keith (2007); Blahak et al. (2010); Baidya Roy (2011); Jacobson and Archer (2012), Fitch et al. (2012 , 2013b), and Abkar and Porté-Agel (2015).

3

Apart from a local drag force, an additional turbulence Kinetic Energy (TKE) source term is assumed in the schemes proposed by Adams and Keith (2007); Blahak et al. (2010); Fitch et al. (2012), and Abkar and Porté-Agel (2015).

In this article we develop a new approach, which is hereafter referred to as Explicit Wake Parametrisation (EWP). We define the TKE from random fluctuations around the ensemble-averaged velocity, instead of around the grid-cell averaged velocity as done in the previous parametrisations. Therefore, to be consistent with the flow equations of the model, we apply a grid-cell averaged drag force and additional TKE is only provided by the PBL scheme where there is an increased vertical shear in horizontal velocity compared to the free-stream velocity profile.

We implemented the EWP scheme in the open source Weather Research and Forecast (WRF) model (Skamarock et al., 2008). The WRF model already includes a wind farm parametrisation option (Fitch et al., 2012; Jiménez et al., 2014), which we will denote as WRF-WF. We validated the WRF-WF and EWP parametrisations against long-term meteorological (met) mast measurements in the wake of an offshore wind farm. To our knowledge, measurements in the wake of a wind farm have not been used for the validation of a wind farm parametrisation model in previous literature.

In Sect. 2, we explain the theoretical basis of the EWP scheme and its implementation in the WRF model. Section 3 describes the measurements, whereas Sect. 4 introduces the WRF model set-up and the configuration of the EWP and WRF-WF scheme. In Sect. 5 both wind farm parametrisations are validated against the met mast measurements in the wake of the wind farm. A discussion of the results finalises the article in Sect. 6, followed by the conclusions in Sect. 7.

2 The Explicit Wake Parametrisation

We start by introducing the relevant mesoscale model equations. Thereafter, the additional terms that represent the effect of the the wind turbines are derived and added to the model

equations. At the end of the section their implementation in the mesoscale model is described.

2.1 The mesoscale model framework

Wind turbines are well described by drag devices that slow down the wind velocity from a free-stream value ~~U~~ u. Downstream, due to mixing of fluid particles from within and outside the wake, the velocity deficit is gradually reduced to the point at which the background conditions are restored.

We use a mesoscale model for the simulation of the wind farm wake and its recovery. It uses the Reynolds Averaged Navier–Stokes (RANS) equations,

$$\frac{\partial U_i}{\partial t}\,\frac{\partial \overline{u}_i}{\partial t} + U_j\frac{\partial U_i}{\partial x_j}\,\overline{u}_j\frac{\partial \overline{u}_i}{\partial x_j} + \frac{\partial \overline{u_i u_j}}{\partial x_j}\,\frac{\partial \overline{u'_i u'_j}}{\partial x_j} = -\frac{1}{\rho}\frac{\partial P}{\partial x_i}\,\frac{\partial \overline{p}}{\partial x_i} - \varepsilon_{i3k}\,f\,U\,\overline{u}_k - \delta_{i3}\,g + F\,\overline{f}_{D\,d_i}, \quad (1)$$

to describe the flow evolution. We ~~We will use the notation and symbols of Wyngaard (2010). The upper-case letters refer to ensemble-averaged quantities, whereas lower-case letters refer to fluctuations.~~ We use an over-line to denote ensemble-averaged quantities and a prime for a fluctuation around the ensemble average. The exception is the average air density $\rho(x,t)$, where t denotes the time and x the position. In Eq. (1), ~~$U_i(x,t)$ and $P(x,t)$~~ $\overline{u}_i(x,t)$ and $\overline{p}(x,t)$ represent the mean velocity components and the pressure, whereas ~~f~~ Ω_j and g are the ~~Coriolis frequency~~ earth's rotation vector and the gravitational acceleration constant. Furthermore, the right most term ~~$F_{D_i}(x,t)$~~ $\overline{f}_{d_i}(x,t)$ is the ensemble-averaged horizontal forcing due to the action of wind turbines (~~$F_{D_3}=0$~~ $\overline{f}_{d_3}=0$).

Mesoscale models generally simulate the effects of turbulence in the vertical direction only. The components of the Reynolds stress are parametrised in a 1.5-order PBL scheme as

$$\overline{u'_i u'_3} = -K_{\mathrm{m}}\frac{\partial U_i}{\partial x_3}\,m\frac{\partial \overline{u}_i}{\partial x_3}, \quad (2)$$

5

where the turbulence diffusion coefficient for momentum, $K_m(\boldsymbol{x},t) = S_m \ell \overline{u_i' u_i'}^{\frac{1}{2}}$, depends on the stability function $S_m(\boldsymbol{x},t)$, the turbulence length scale $\ell(\boldsymbol{x},t)$, and the TKE per unit mass $\overline{u_i' u_i'}/2$. We write the most general form of the TKE equation:

$$\frac{\partial \overline{e}}{\partial t} + \overline{T} = \overline{p}_s + \overline{p}_b + \overline{p}_t - \epsilon, \tag{3}$$

where on the left hand side (l.h.s.) $\overline{e}$ denotes the TKE and $\overline{T}$ the transport, which includes the advection by the mean flow, turbulence transport of TKE and the divergence of the pressure correlation. On the right hand side (r.h.s.), $\overline{p}_s$ represents the turbulence production from the vertical shear in the horizontal velocity (shear production), $\overline{p}_b$ the turbulence production or destruction related to buoyancy forces, $\overline{p}_t$ the turbulence induced by the turbine rotor, and ϵ the dissipation.

2.2 The mesoscale model grid

For the mesocale model, the previously defined variables in the Eqs. (1) and (3) have to be redefined on the three-dimensional model grid.

A new volume-averaged velocity equation is derived by integrating Eq. (1) over the grid-cell volume. For Eq. (3), we define a (random) velocity fluctuation at any hypothetical measurement point within a grid-cell volume to be the difference between the ensemble-averaged and the instantaneous velocity. This is illustrated schematically in Fig. 1a. Then, the grid-cell averaged TKE can be thought of as the variance of the velocity fluctuations around the ensemble-averaged velocity and not around the grid-cell averaged velocity as shown in Fig. 1b.

The aim is to obtain expressions for the terms P_t (Eq. 3) and F_D (Eq. 1) that are consistent with the mesoscale model flow equations. The expression for Pt can be found by multiplying the Navier–Stokes equations with the velocity fluctuation and then applying Reynolds

averaging. This gives for the additional source term:

$$P_{\mathsf{t}} = \overline{\rho\,A_{\mathsf{r}}\,c_{\mathsf{T}}\,(U_i + u_i)^2\,u_i}/2 \sim \rho\,A_{\mathsf{r}}\,C_{\mathsf{T}}\,U\overline{u_i^2}, \tag{4}$$

where $\rho\,A_{\mathsf{r}}\,c_{\mathsf{T}}\,(U_i + u_i)^2$ is the instantaneous forcing due to the action of the wind turbine, the lower case c_T the instantaneous thrust coefficient, the upper case C_T the averaged thrust coefficient, and Ar the rotor area. This additional turbulence occurs directly behind the turbine blades. Its turbulence length scale ℓ is expected to scale with the blade's cord length, which is on the order of a few metres and it is therefore much smaller than that of the atmospheric flow. The smaller length scale implies a significant higher dissipation rate $\epsilon \propto (1/\ell)\overline{u_i u_i}^{3/2}$. Therefore, we assume the source term in Eq. (4) to dissipate within a mesoscale model grid-cell and neglect P_{t} of Eq. (4) on the grid-cell average. Additional turbulence is generated by shear production, which we assume to be the dominant mechanism on the grid-cell average. In the following sections, we derive the expression for the grid-cell averaged F_D.

For the parametrisation, we aim to obtain expressions for the volume-averaged drag force, $\langle \overline{f_d} \rangle$, and the averaged turbulence induced by the turbine, $\langle \overline{p_t} \rangle$ that are consistent with the mesoscale model flow equations. Here, the angle brackets denote the volume average.

A new volume-averaged velocity equation is derived by integrating Eq. (1) over the grid-cell volume. This gives the expression for $\langle \overline{f_d} \rangle$, which is derived in the following Sect. 2.2.1.

The derivation of the additional term $\langle \overline{p_t} \rangle$ depends on the definition of the velocity perturbation. Formally, a velocity perturbation is the difference between the instantaneous and ensemble-averaged velocity. For homogeneous flows, the spatial-averaged velocity can be used for the definition of a velocity fluctuation, since the ensemble average can be approximated by the spatial average. However, the flow around wind turbines is

7

non-homogeneous and consequently the spatial and ensemble average deviate. This has been illustrated in Fig. 1. Double averaging (ensemble and spatial) allows to separate the total kinetic energy into three components. The definition of the term $\langle \overline{p}_t \rangle$ in the TKE equation will then depend on which of the three components contribute to the mean and which to the turbulence kinetic energy. In Appendix A, we discuss in more detail the double averaging and the ways mean and turbulence kinetic energy can be described.

In the EWP scheme, we follow Raupach and Shaw (1982) and Finnigan and Shaw (2008) and define a turbulence fluctuation around the ensemble mean (Approach I in Appendix A). Therefore, we include only the random motion in the TKE. With this definition, the additional term becomes $\langle \overline{p}_t \rangle = \langle \overline{u'_{i,h} f'_{d_i}} \rangle$, where h is the hub-height of the turbine. When we use for the drag force, $f_{d_i} = -\rho A_r c_t u_{i,h}^2 / 2$, where $c_t(u)$ is the thrust coefficient and A_r the rotor area, we obtain:

$$\langle \overline{p}_t \rangle = \langle \overline{u_{i,h} f_{d_i}} \rangle - \langle \overline{u}_{i,h} \overline{f}_{d_i} \rangle$$

$$= -\rho A_r c_t \langle \overline{(\overline{u}_{i,h} + u'_{i,h}) u_{i,h}^2} \rangle / 2 + \rho A_r c_t \langle \overline{u}_{i,h} \overline{u_{i,h}^2} \rangle / 2$$

$$\approx -\rho A_r c_t \langle \overline{u}_{i,h} \overline{u'^2_{i,h}} \rangle, \tag{4}$$

This term represents a sink of TKE due to the extraction of momentum. The magnitude of this term is much smaller than the additional term in the WRF-WF scheme (see Sect. 4.1.2). Therefore, the additional term $\langle \overline{p}_t \rangle$ is neglected in the EWP approach. Additional turbulence is generated by shear production, which we assume to be the dominant mechanism on the grid-cell average. In the following sections, we derive the expression for the grid-cell averaged $\langle \overline{f}_d \rangle$.

8

2.2.1 The sub-grid wake expansion

The velocity deficit expansion in the vertical direction within one grid-cell is not negligible, which leads to flow decelerations that extend beyond the rotor swept area. This part of the wake expansion is not accounted for in the mesoscale model, hence we estimate it explicitly with a sub-grid scale (turbulence) diffusion equation. Then, a grid-cell averaged force is determined and added to the model RANS equations.

~~The sub-grid-scale model describes the unresolved turbulence diffusion process that results from turbulence shear production.~~ In this model, we assume the horizontal advection of velocity and the turbulence diffusion to dominate in Eq. (1). Considering first only the flow behind the turbine rotor, we obtain from Eqs. (1) and (2) the diffusion equation:

$$U_0\overline{u}_o \frac{\partial}{\partial x}\left(U_0\overline{u}_o - \widehat{u}\right) = K\frac{\partial^2}{\partial z^2}\left(U_0\overline{u}_o - \widehat{u}\right) + K\frac{\partial^2}{\partial y^2}\left(U_0\overline{u}_o - \widehat{u}\right) \tag{5}$$

that describes the expansion of the velocity deficit, $\overline{U_0 - \widehat{U}}\,\overline{u}_o - \widehat{u}$, behind the turbine. ~~Here, we denote the advection velocity at hub-height h by $U_0 = |U(h,t)|$ and the unresolved velocity in the stream-wise direction x in the wake of the turbine by $U(x)$.~~ Here, $\overline{u}_o = |\overline{u}(h,t)|$ denotes the advection velocity at hub-height and $\widehat{u}(x)$ the unresolved velocity in the stream-wise direction x in the wake of the turbine. The turbulence diffusion, which causes the wake expansion, is described by a single turbulence diffusion coefficient ~~$K = K_m(h,t)$~~ $K = K_m(x,y,h,t)$ in Eq. (2) and is given by the PBL scheme in WRF.

2.2.2 The velocity deficit profile

We define the vertical structure of the velocity deficit as ~~$U_d = U_s\xi$, where $U_s(x)$~~ $\overline{u}_d = \overline{u}_s\xi$, where $\overline{u}_s(x)$ is the maximum velocity deficit at the centre of the wake and $\xi(x,y,z)$ a function that determines the ~~vertical~~ wake ~~extension~~ expansion (Tennekes and Lumley, 1972).

9

Equation (5) can be solved for the velocity deficit profile:

$$U_{\mathrm{d}}\overline{u}_d = U_{\mathrm{s}}\overline{u}_s \exp\left[-\frac{1}{2}\left(\frac{z-h}{\sigma}\right)^2 - \frac{1}{2}\left(\frac{y}{\sigma}\right)^2\right], \tag{6}$$

where the length scale, σ, that determines the ~~vertical~~ wake ~~extension~~ expansion is

$$\sigma^2 = \frac{2\,K}{U_0}\frac{2\,K}{\overline{u}_0}\,x + \sigma_0^2. \tag{7}$$

5 ~~In Eq. (7), σ_0 denotes the initial length scale. Equation (7) represents the vertical wake extension, resulting from turbulent diffusion of momentum and it is similar to the solution of Eq. (4.29) in Wyngaard (2010) for the dispersion of plumes. Equation (6) describes the ensemble-averaged profile of the velocity deficit around hub-height at a given point in the far turbine wake (Tennekes and Lumley, 1972). The turbine wake is normally divided~~

10 ~~in a near and far wake, where the far wake begins between one rotor diameter D0 (Vermeer et al., 2003) and 3 D0 (Crespo and Hernández, 1996).~~ Equation (6) describes the ensemble-averaged profile of the velocity deficit around hub-height at a given point in the far wake (Tennekes and Lumley, 1972). Equation (7) represents the vertical wake extension, resulting from turbulent diffusion of momentum and it is similar to the solution of Eq. (4.29)

15 in Wyngaard (2010) for the dispersion of plumes. Normally, the turbine wake is divided into a near and far wake, where the far wake begins between 1 and 3 rotor diameters (Vermeer et al., 2003 and Crespo and Hernández, 1996). In the parametrisation, we account for the near wake expansion in the initial length scale σ_0 and describe the unresolved far wake expansion with Eq. (6). We can find the velocity deficit profile for wind turbines by equating

20 the total thrust to the momentum removed by the action of the wind turbine, i.e.,

$$\frac{1}{2}\rho\,C_{\mathrm{T}}c_t\,\pi\,R_0 r_0^2\,U_0\overline{u}_0^2 = \int\limits_{-\infty}^{\infty}\int\limits_{-\infty}^{\infty} \rho\,U_0 U_{\mathrm{d}}\overline{u}_0\overline{u}_d\,\mathrm{d}z\,\mathrm{d}y = \rho\,U_0\overline{u}_0\,U_{\mathrm{s}}\overline{u}_s 2\,\pi\,\sigma^2, \tag{8}$$

10

where $C_T(U_0)$ is the turbine thrust coefficient and R_0 the r_o is the radius of the rotor. In Eq. (8), the l.h.s. represents the local forces at the rotor swept area, whereas the r.h.s. describes the equivalent distributed force for the expanded wake at any x. From the Eqs. (8) and (6), we find the velocity deficit profile for a specific thrust force,

$$U_d \overline{u}_d = \frac{C_T R_0^2 U_0}{4\sigma^2} \frac{c_t r_o^2 \overline{u}_o}{4\sigma^2} \exp\left[-\frac{1}{2}\left(\frac{z-h}{\sigma}\right)^2 - \frac{1}{2}\left(\frac{y}{\sigma}\right)^2\right]. \qquad (9)$$

When we insert the velocity deficit of Eq. (9) in the second term of Eq. (8) and integrate in the cross-stream direction y, we have the integrated thrust profile

$$F_D \overline{f}_d = \int_{-\infty}^{\infty} \int_{-\infty}^{\infty} \rho U_0 U_d \overline{u}_o \overline{u}_d \, dz \, dy = \int_{-\infty}^{\infty} \rho \sqrt{\frac{\pi}{8}} \frac{C_T R_0^2 U_0^2}{\sigma} \frac{c_t r_o^2 \overline{u}_o^2}{\sigma} \exp\left[-\frac{1}{2}\left(\frac{z-h}{\sigma}\right)^2\right] dz. \qquad (10)$$

The term on the r.h.s. within the integral describes the equivalent distributed thrust force in the vertical direction at any distance x. Next, we derive from Eq. (10) a single effective thrust force, which represents the average wake expansion within a grid-cell.

2.2.3   Turbine forcing in the mesoscale model

For the mesoscale model we derive an effective thrust force, which describes the average wake expansion within a grid-cell. Therefore, we first determine the effective velocity deficit profile $U_e \overline{u}_e$ by averaging the velocity deficit of Eq. (9) over the cross-stream direction y and over a downstream distance L that the wake travelled within the grid-cell. It is convenient to approximate this area-averaged velocity deficit profile by a Gaussian-shaped profile:

$$U_e \overline{u}_e = \sqrt{\frac{\pi}{8}} \frac{C_T R_0^2 U_0^2}{\sigma_e} \frac{c_t r_o^2 \overline{u}_o}{\sigma_e} \exp\left[-\frac{1}{2}\left(\frac{z-h}{\sigma_e}\right)^2\right] \cong \frac{1}{L} \int_0^L \int_{-\infty}^{\infty} U_d \overline{u}_d \, dy \, dx. \qquad (11)$$

11

~~see Appendix~~ In Appendix B, we compare the area-averaged velocity deficit profile to the approximated Gaussian-shaped profile. Here σ_e is the effective length scale that is related to the model grid-size,

$$\sigma_e = \frac{1}{L} \int_0^L \sigma \, dx = \frac{U_0}{3\,K\,L} \frac{\overline{u}_\mathrm{o}}{3\,K\,L} \left[\left(\frac{2\,K}{U_0} \frac{2\,K}{\overline{u}_\mathrm{o}} L + \sigma_\mathrm{o}^2 \right)^{\frac{3}{2}} - \sigma_\mathrm{o}^3 \right]. \tag{12}$$

From the definition of the effective length scale, we can obtain the total effective thrust force ~~F_e~~ $\overline{f}_e$ by substituting the length scale σ in Eq. (10), with the effective length scale σ_e. This gives

$$F_\mathrm{e}\overline{f}_e = \int_{-\infty}^{\infty} \rho \sqrt{\frac{\pi}{8}} \frac{C_\mathsf{T}\,R_0^2\,U_0^2}{\sigma_\mathsf{e}} \frac{c_r\,r_\mathsf{o}^2\,\overline{u}_\mathsf{o}^2}{\sigma_e} \exp\left[-\frac{1}{2}\left(\frac{z-h}{\sigma_e} \right)^2 \right] dz. \tag{13}$$

The grid-cell averaged acceleration for the model RANS equations, Eq. (1), is now obtained, when we divide Eq. (13) by the mass and apply the grid-cell volume. For every vertical model layer k, we obtain then from Eq. (13) the grid-cell averaged acceleration components,

$$\langle F_{D_1}\overline{f}_{d_1}(k) \rangle = -\sqrt{\frac{\pi}{8}} \frac{C_\mathsf{T}\,R_0^2\,U_0^2}{\Delta x\,\Delta y\,\sigma_\mathsf{e}} \frac{c_t\,r_\mathsf{o}^2\,\overline{u}_\mathsf{o}^2}{\Delta x\,\Delta y\,\sigma_e} \exp\left[-\frac{1}{2}\left(\frac{z-h}{\sigma_e} \right)^2 \right] \cos[\varphi(k)] \tag{14}$$

and

$$\langle F_{D_2}\overline{f}_{d_2}(k) \rangle = -\sqrt{\frac{\pi}{8}} \frac{C_\mathsf{T}\,R_0^2\,U_0^2}{\Delta x\,\Delta y\,\sigma_\mathsf{e}} \frac{c_t\,r_\mathsf{o}^2\,\overline{u}_\mathsf{o}^2}{\Delta x\,\Delta y\,\sigma_e} \exp\left[-\frac{1}{2}\left(\frac{z-h}{\sigma_e} \right)^2 \right] \sin[\varphi(k)] \tag{15}$$

in the x and y direction, respectively. In Eqs. (14) and (15), we use Δx and Δy for the horizontal grid-spacing in the x and y direction, $\varphi(k)$ for the wind direction, and the angular brackets for the spatial averaging. For the height $z(k)$, we use the height at the centre of layer k.

2.3   Implementation in the WRF model

We assume every turbine within a grid-cell to be positioned at its centre and use $L = \Delta x/2$ in Eq. (12). ~~For each turbine a thrust force is calculated with Eqs. (14) and (15). The total thrust force for a turbine containing grid-cell is then obtained from a superposition of the single turbine thrust forces and is added to the numerical approximation of Eq. (1).~~ In the numerical model, Eqs. (14) and (15) are added to the numerical approximation of Eq. (1). Furthermore, Eq. (12) is used to determine the effective length scale σ_e of the vertical wake extension. At every time-step the total thrust force within a grid-cell is obtained from a superposition of the single turbine thrust forces.

~~We use the grid-cell averaged velocity as the upstream velocity U0 to the wind turbine (see Sect. 6).~~ To a first approximation, we use the grid-cell averaged velocity at hub-height, $\langle \overline{u}_{\mathrm{o},h} \rangle$ as the upstream velocity $\overline{u}_{\mathrm{o}}$ for all turbines within the same grid-cell (see Sect. 6). The turbulence diffusion coefficient for momentum, K in Eq. (12), comes from the selected PBL scheme. The parametrisation, therefore, can be used with any PBL scheme. However, to be consistent with the assumptions used in the derivation of the wind farm parametrisation, a ~~second~~ 1.5 order closure scheme with a turbulence shear production term is recommended. A practical description of how to use the EWP scheme in the WRF model is given in ~~Sect. 7.~~ the section "Code availability" at the end of the paper.

3   Wind farm and measurements

3.1   The Horns Rev I wind farm and met masts

The parallelogram-shaped Horns Rev I wind farm is situated in the North Sea about 15 km West of the Danish coast (Fig. 2). It is made up of 80 Vestas V80 (2 MW) pitch controlled, variable speed turbines, resulting in a total rated wind farm capacity of 160 MW. The turbines have a swept area diameter of 80 m with the hub mounted at 70 m a.m.s.l. The equally-

spaced turbines are placed in 10 columns from West to East and 8 rows from North to South, labelled C1–C10 and R1–R8 in Fig. 2b. The spacing between columns and rows is 560 m, which is equivalent to 7 turbine diameters. Hansen et al. (2012) describes in detail the various production data available at the wind farm, their quality filtering, and processing.

Turbine (C1,R7) is used as a reference turbine, since it is not affected by the wind farm wake under westerly flows; in Fig. 2b it is marked with the solid bullet. The wind speed for each turbine is estimated from the power production data, using the turbine specific power curve and the wind direction is obtained from the adjusted yaw angle (Hansen et al., 2012).

For the validation, we use data from two met masts, M6 and M7, whose positions are shown in Fig. 2b. The masts are located 2 and 6 km to the east of the eastern edge of the wind farm and are thus directly in its wake for westerly winds. The 70 m̶ m tall masts are identically equipped and their instrumentation includes high quality Risø cup anemometers for measuring wind speeds. The 10-min averaged data from the two masts, which are independent of the wind farm data, is used to validate the modelled wind speed reductions downstream from the wind farm.

3.2 Data selection and averaging for the validation

For the validation of the results of the model simulations, and especially because of the relatively large area-averaged fields in the mesoscale model, it is very important to ensure that measurements and model fields are comparable. This can be achieved by properly selecting the wind direction and wind speed interval at the reference turbine.

Regarding the wind direction selection, Gaumond et al. (2013) found at Horns Rev I, for narrow wind direction sectors, a higher measured turbine production compared to that estimated by wake models. Most likely this is related to wind direction variations, which, for small wind direction bins, exceed the bin size within the 10 min averaging period. Since these variations are not accounted for in the model, we follow the recommendation to average over a relatively large wind direction interval. Furthermore, it is important that the flow reaching the mast anemometers has passed through the wind farm, otherwise it does not characterise the wind farm wake. Therefore, we select velocities whose directions are at

14

the reference turbine between 255 and 285°. As demonstrated in Fig. 2b, the flow from this sector is influenced by the wind farm wake.

In the period 2005 to 2009, we select the 10-min averaged wind speeds from 6.5 to 11.5 ~~m~~ m s^{-1} at the reference turbine and bin them in 1 ~~m~~ m s^{-1} intervals. In this range, we guarantee to be above the cut-in wind speed of the turbines (4 m s^{-1}) and below the wind speed at which the control system starts to pitch the blades (13 m s^{-1}). To obtain as much data as possible, we do not filter the measurements on stability. For strong westerly winds, we expect the ~~lower~~ atmospheric stability near to the ground on average to be neutral (Sathe et al., 2011).

For every instance that the wind direction and wind speed at the reference turbine was within the above described range, the wind speeds at M6 and M7 were accepted. Afterwards, the selected wind speeds were averaged for each wind speed bin and normalised by the average wind speed at the reference turbine $\overline{U_\mathrm{ref}}$ $\overline{u}_\mathrm{ref}$ (Table 1).

4 WRF model configuration and averaging

In the simulations we used the WRF model V3.4. However, the WRF-WF parametrisation has been updated to the version available in WRFV3.6. The model domain is set-up with 80×40 grid-cells, with a horizontal grid-spacing $\Delta x = \Delta y = 1120\,\mathrm{m}$. This horizontal grid-spacing, which is twice the turbine separation, guarantees a constant number of turbines per grid-cell in the flow direction. Equally to the Horns Rev I wind farm, the model wind farm contains 80 V80 turbines and extends over 5 grid-cells in the West–East and North–South direction (Fig. 3a). The Vestas V80 thrust and power curves were used for the turbine parameters.

The model was run in an idealised case mode with open lateral boundary conditions (Skamarock et al., 2008, p. 51), Coriolis forcing and zero heat fluxes from the lower boundary. At the surface, the no slip condition holds. ~~The surface roughness was constant in time and set to $z_0 = 2 \times 10^{-4}$ m for the entire domain.~~ The total domain is located over water and we prescribe a constant roughness length of $z_0 = 2 \times 10^{-4}$ m, which follows the World

15

Meteorological Organization (WMO) standards. The friction velocity is obtained with the Charnock formula. The model simulations were run with the MYNN 1.5 order Level 2.5 PBL scheme (Nakanishi and Niino, 2009), on which the WRF-WF scheme is dependent. These and other details of the model configuration are summarised in Table 2.

5   We ran simulations for 5 wind speed intervals and for 9 wind directions, ranging from 255 to 285°. Additionally, to investigate a the sensitivity to the vertical resolution, we set-up three experiments with 40 (L40), 60 (L60), and 80 (L80) layers in the vertical direction. With these vertical resolutions there are 5, 7, and 10 grid-cell volumes intersecting with the turbine rotor as shown in Fig. 3b.

10   All 135 simulations (5 wind speeds, 9 wind directions, and 3 vertical resolutions) were initialised with a constant geostrophic wind in height in a dry and slightly stable atmosphere. After a four day integration period, the wind converged in the whole domain to a logarithmic neutral profile within a 650 m deep boundary layer and remained independent of height above. The boundary layer was capped by an inversion layer with a potential temperature 15 gradient of around 6 K km^{-1}. Above the inversion layer the velocity remained independent of height. The atmospheric state of each of these 135 simulations was used to drive: a control simulation without wind farm parametrisation, a simulation with the WRF-WF scheme, and a simulation with the EWP scheme. We used the restart option in the WRF model to initialise these simulations.

20   Each control or wind farm simulation lasted one day, resulting in a total simulation length of five days. The wind speeds in the control simulations were 7, 8, 9, 10, and 11 m s^{-1} at 70 m (hub-height) after 5 days of simulation. We ended up with the desired magnitude of the geostrophic wind by conducting several experiments with different initialisations.

   To summarise, we performed simulations for 9 wind directions, 5 wind speeds, and 3 25 vertical resolutions, with and without wind farm parametrisation, which gives a total of 405 (3 times 135) simulations as outlined in Table 3. For the validation against the mast measurements, we averaged the model wind speeds over the 9 wind directions with a uniform direction distribution. We used the instantaneous wind speeds at the end of the simulation period for the validation. Similarly to the observations, we normalise the wind direction aver-

16

aged wind speeds and hereafter simply refer to them as "velocity". The model wind speeds from the simulations without the wind farm were used to normalise the wind farm flow.

4.1 Wind farm parameters

4.1.1 The EWP scheme

We use the wind speeds, derived from the power production data of the turbines, to determine the initial length scale σ_o in Eq. (12). To a first approximation the initial length scale is defined to be independent of the upstream conditions and it is therefore the same for all turbines. The initial length scale is assumed to scale with the rotor radius and accounts for the near wake expansion.

For this calibration, we selected turbine production data at time stamps when the derived upstream wind speed and wind direction at the reference turbine ranged from 8.5 to $9.5\,\mathrm{m\,s^{-1}}$ and from 255 to $285°$. This wind speed bin was selected, since it contains the most turbine observations. It has a minimum of 850 observations for a turbine at the eastern edge of the wind farm and a maximum of 1612 observations for a turbine in the first wind farm column. The difference in the selected number of observations results from the additional requirement that for a given turbine the local upstream turbines have to be operational, in order to guarantee wake losses. For the power production data obtained in this way, we used the power curve to derive the wind speed. The column averaged velocity was afterwards obtained by averaging over the inner 6 rows (R2–R7). The outer rows were excluded because they experience different wake conditions under various wind directions.

Similarly to the model experiments in Sect. 4, we performed simulations for 9 wind directions between 255 to $285°$ for the 3 vertical resolutions with a wind speed at hub-height of $9\,\mathrm{m\,s^{-1}}$. ~~Additionally~~ To determine the best fitting value, we varied for the EWP simulations the initial length scale for all turbines from ~~$\sigma_0 = R_0$ to $\sigma_0 = 2R_0$~~ $\sigma_o = r_o$ to $\sigma_o = 2r_o$, stepping with ~~$\Delta R_0 = 0.1$~~ $\Delta r_o = 0.1$~~, to determine the best fitting value~~. For the comparison to the measurements, the column-averaged wind speed was obtained by averaging over the 3 central wind farm grid-cells in the cross-stream direction.

17

~~Figure 4 shows~~ The lines in Fig. 4 show ~~the results~~ the hub-height velocity from the simulations with $\sigma_0 = 1.7 R_0$ $\sigma_0 = 1.7 r_0$, which had the smallest overall bias compared to the measurements. Additionally, the coloured dots indicate the sensitivity to the initial length scale for $\sigma_0 = 1.5$ and $1.9 r_0$. It shows the same velocity reduction for all 3 vertical resolutions. Consequently, the amount of energy extracted by the turbines is independent of the vertical resolution. The simulations with an initial length scale $\sigma_0 = 1.7 R_0$ $\sigma_0 = 1.7 r_0$ follow the measured velocity reduction fairly well. ~~Therefore, we conclude that for neutral conditions the initial length scale can assumed to be independent of the upstream conditions.~~ We use this length scale for all simulations in Sect. 5.

4.1.2 The WRF-WF scheme

In the validation, we also include results from the wind farm parametrisation WRF-WF from WRF-V3.6. This parametrisation was introduced in ~~WRFV3.4~~ WRFV3.3 by Fitch et al. (2012). In this approach, a forcing term F_D is applied to every model level that intersects with the wind turbine blade sweep area and thus the scheme simulates the local drag forces over the turbine rotor. The additional TKE source term is parametrised as

$$P_{t,\text{WRF-WF}} = \rho A_r (C_T - C_P) U^3 / 2, \tag{16}$$

$$\langle \bar{p}_{t,\text{WRF-WF}} \rangle = \rho A_r (c_t - c_p) \langle \overline{|u|} \rangle^3 / 2, \tag{16}$$

here ~~C_T and C_P are the thrust and power coefficients~~ c_p is the power coefficient of the turbine, whereas ~~U is the grid-cell velocity~~ $\langle \overline{|u|} \rangle$ the absolute value of the grid-cell velocity. The application of one-dimensional theory (Hansen, 2003) on Eq. (16), gives ~~$P_{t,\text{WRF-WF}} = \rho A_r C_T a U^3 / 2$~~ $\bar{p}_{t,\text{WRF-WF}} = \rho A_r c_t a \langle \overline{|u|} \rangle^3 / 2$ for the additional TKE term. Here, a denotes the induction factor.

The same result, ~~$P_{t,\text{WRF-WF}} = \rho A_r C_T a U^3 / 2,$~~ ~~can~~ ~~also~~ ~~be~~ $\langle \bar{p}_{t,\text{WRF-WF}} \rangle = \rho A_r c_t a \langle \overline{|u|} \rangle^3 / 2,$ is obtained by defining a velocity fluctuation as the

18

difference between the grid-cell averaged velocity and the instantaneous velocity ~~as illustrated in Fig. 1b.~~ (Approach II in Appendix A). In Fig. 1, this velocity fluctuation has been denoted by u''. ~~This has been analytically derived by~~ An analytical derivation can be found in Abkar and Porté-Agel (2015) (their Eq. 21, with their $\xi = 1$). In this definition of TKE, the turbine induced velocity reduction is counted as TKE. ~~The TKE source term from the WRF-WF scheme in Eq. (16) is much larger than the source term in Eq. (4)~~ For the considered wind speeds the absolute value of $\langle \overline{p}_{t,\text{WRF-WF}} \rangle$ is around 30 times larger than $\langle \overline{p}_t \rangle$ defined in Eq. (4), which comes from the different definition of TKE in the two schemes. For example, for $10\,\text{m s}^{-1}$ with $c_t = 0.79$, $c_p = 0.43$, and $\langle \overline{u_{i,h}'^2} \rangle = 0.7\,\text{m}^2\,\text{s}^{-2}$ at hub-height, the ratio between $\langle \overline{p}_{t,\text{WRF-WF}} \rangle$ and $\langle \overline{p}_t \rangle$ as it has been defined in Eq. (4) is 32.

In ~~WRFV3.4, the~~ Sect. 5, we use the up-dated WRF-WF parametrisation ~~the power coefficient has been obtained from the power curve information. The thrust coefficient was then determined by an empirical relationship with the power coefficient. improved the performance of the WRF-WF scheme in a comparison against turbine measurements of the Horns Rev I wind farm by using both a turbine thrust and power coefficient. This approach is used in the experiments performed in Sect. 5.~~ from WRFV3.6, which has no free parameters. The power and thrust coefficients come from the Vestas V80 turbine.

5 Validation of the wind farm parametrisations

To obtain a complete picture of the modelled velocity field within and downstream of the Horns Rev I wind farm, we ~~compare the hub-height velocity simulated by the WRF model using the two wind farm parametrisations for one wind speed bin. We used the second most frequently observed wind speed bin ($10\,\text{m s}^{-1}$), which is different from that used in the calibration (Sect. 4.1.1), to be as calibration independent as possible. Afterwards, we compare the modelled velocities for all wind speed to the measurements at M6 (2 km downstream) and M7 (6 km downstream).~~ compare: (I) the velocity decay in the wake of the wind farm from the two wind farm parametrisations to the measurements for the $10\,\text{m s}^{-1}$ wind speed bin. (II) the modelled velocities to the measurements at M6 (2 km downstream)

19

and M7 (6 km downstream) for all five wind speeds (7, 8, 9, 10, and 11 m s^{-1}). We recall that the initial length scale used in the EWP scheme has been determined for 9 m s^{-1}.

In a qualitative validation, we examine the ~~simulated wind farm wake characteristics, as well as~~ velocity reduction behind the wind farm and the profile of the ~~wake deficits, using results from~~ velocity deficit. Furthermore, we discuss the vertical structure of the modelled TKE field from the discretized Eq. (3), where the additional term $\langle \overline{p_t} \rangle$ has been parametrised in the WRF-WF scheme and neglected in the EWP scheme. We use results from independent LES simulations and wind tunnel experiments as a ~~-~~reference.

In the validation, we use the instantaneous model outputs from the converged flow field after the 5 days integration period. Furthermore, the velocities are normalised as described in the Sects. 3 and 4.

5.1 Velocity recovery at turbine hub-height

Figure 5 shows the wind direction averaged hub-height velocity (10 m s^{-1} bin) as a function of the downstream distance for the EWP and WRF-WF schemes and all vertical resolutions. For the EWP scheme (Fig. 5a) there is no identifiable vertical resolution dependency on the velocity, while for the WRF-WF (Fig. 5b) this is small. ~~In the EWP scheme the velocity within the wind farm decreases almost linearly with distance, whereas for the WRF-WF scheme, after a more rapid initial decrease, the velocity becomes nearly constant with distance at the end of the wind farm.~~ In the EWP scheme the velocity within the wind farm decreases almost linearly with distance. On the other hand, in the WRF-WF scheme it decreases more rapidly in the first turbine columns and becomes nearly constant with distance at the end of the wind farm. The behaviour in the EWP scheme suggests that no equilibrium has been reached within the wind farm between the extracted momentum by the wind turbines and the compensating flux of momentum from above. On the other hand, from the nearly constant velocity at the end of the wind farm for the WRF-WF scheme, it seems that the extraction of momentum by the turbines is almost balanced by the flux of momentum from aloft. At the end of the wind farm the velocity difference between the two schemes is only 0.1 %. We have indicated the velocity from the EWP scheme at the most easterly grid-cell

20

of the wind farm with a dotted horizontal line in Fig. 5. This agreement is noteworthy, given the two different methods used. ~~However, the velocity 2 km downstream of the wind farm, at M6, differs between the schemes by 4.7%. This means that downstream of the wind farm grid-cells, where the wind farm parametrisations are not active, the velocity diverges for the two schemes and the difference becomes significant. This is important, especially if it~~ At M6, 2 km downstream of the wind farm, the modelled velocity for both schemes is within the uncertainty of the measurements. Nevertheless, the difference between the schemes is increased from 0.1 % at the end of the wind farm to 4.7 % at M6. This means that downstream of the wind farm grid-cells, where the wind farm parametrisations are not active, the velocity diverges for the two schemes and the difference becomes significant. The near wake recovery is important, especially if the velocity was used to estimate the power production on a neighbouring wind farm that was located at this distance from the original wind farm. For example, the Rødsand 2 and Nysted offshore wind farm in Southern Denmark are separated by a comparable distance.

Figure 6 depicts wind direction averaged velocity recovery at the two met masts for all 5 wind speed bins and all vertical resolutions. It shows the differences in the WRF-modelled and measured wind speed at M6 (circles) and M7 (triangles), against the measured wind speed at the same masts. The WRF-modelled wind speed is obtained from linear interpolation of the wind speeds in the nearest grid-cells. The modelled recovery rate can be deduced from the slopes of the solid (between the values at M6 and M7) and dashed lines (between M7 and the free-stream velocity). A negative slope is linked to a slower modelled recovery compared to that measured, whereas a positive slope shows a faster modelled recovery. There is no vertical resolution dependency for a wind farm parametrisation when the circles or triangles for a given wind speed bin lie on top of each other.

The results show that the bias in velocity between the measurements and the EWP simulations is small ($< 0.15\,\mathrm{m\,s^{-1}}$) for all wind speeds (except for the $7\,\mathrm{m\,s^{-1}}$ bin at M7). For the EWP scheme, we find a positive velocity difference at M6 and a negative one at M7. Hence, the modelled wake recovery oscillates between being slightly slower from M6 to M7 and being slightly faster from the end of the wind farm to M6, as well as from M7 to the

21

end of the wake. The velocity of the EWP scheme at M6 is nearly ~~resolution independent~~ independent of the vertical resolution and at M7 the dependency is very weak.

The WRF-WF scheme shows a ~~positive bias~~ positive difference in velocity of up-to 0.5 m s^{-1} at M6. This ~~positive bias~~ difference, between the WRF-WF scheme and the measurements, becomes larger with increasing wind speed. The ~~bias~~ higher modelled velocity at M6 is a consequence of the ~~too fast modelled wake recovery~~ more rapid recovery of the modelled wake compared to that of the measurements from the end of the wind farm to M6. Between M6 and the point at which the free-stream velocity is reached again, the modelled wake recovery is slower than that measured. This overall positive ~~bias implies~~ difference suggests that the modelled velocity with the WRF-WF scheme is overestimated throughout the whole wake.

Figure 7 shows the spatial structure of the modelled velocity (10 m s^{-1} bin) within and in the wake of the wind farm for the L60 simulations in the 270° wind direction. A comparison of the results from the two schemes confirms the faster initial wind farm wake recovery in the WRF-WF scheme. The 10 % velocity deficit contour, for example, extends for the EWP scheme to around $x = 15$ km (Fig. 7a), while for the WRF-WF scheme to $x = 8$ km (Fig. 7b). The difference in the distance at which a 7.5 % velocity deficit is reached is even larger: after $x = 21$ and $x = 11$ km for the EWP and WRF-WF scheme, respectively. Further downstream, after around 30 km, the velocity fields from the two parametrisations become similar. Possible reasons for the difference in the initial wake recovery are discussed in the next section.

Finally, Fig. 7 shows a difference in the orientation of the axis of the velocity deficit downstream from the wind farm. In both simulations the steady-state wind direction of the free-stream flow was 270°. As the velocity decreases within the wind farm, the velocity is expected to turn to the North, due to the changed Coriolis force. In the wind farm wake, where the flow accelerates again, the velocity should turn back again to the background direction. This effect is seen for the EWP scheme (Fig. 7a). Whereas, for the WRF-WF scheme (Fig. 7b) the wake turns southward behind the wind farm. A possible reason for this unexpected behaviour is the turbulence transport of momentum from aloft (Ekman spiral) within

22

the wind farm. In the wind farm wake the flow keeps turning to the South because of the flow acceleration from the momentum transport.

5.2 Vertical profile of TKE and velocity

To obtain a broader understanding of the mechanisms acting in the two schemes, we compare the simulated TKE (per unit mass) and the velocity deficit profiles for the $10\,\mathrm{m\,s^{-1}}$ wind speed bin in the $270°$ wind direction.

Figure 8 shows the difference in TKE (wind farm minus control simulation) for the L60 simulation. The cross-sections in the x, z plane are in the West–East direction and pass through the centre of the wind farm. We used different colour scales in the two plots, due to the relatively large differences in TKE production between the two schemes. However, we have kept the outermost contour ($0.02\,\mathrm{m^2\,s^{-2}}$) the same. The maximum TKE difference was 0.30 and $1.9\,\mathrm{m^2\,s^{-2}}$ for the EWP and WRF-WF scheme, respectively.

Compared to the environmental TKE of the pure shear flow (not shown), the TKE increases in the EWP scheme (Fig. 8a) at the end of the wind farm by a factor of 2, whereas in the WRF-WF scheme (Fig. 8b) it increases at hub-height by a factor of 5.5. The EWP scheme shows an increased and decreased TKE above and below hub-height compared to the reference simulation. The maximum increase occurs behind the wind farm, where the velocity gradients are the largest. In the WRF-WF scheme, the maximum TKE increase happens at hub-height within the wind farm. Recalling that in the WRF-WF scheme, turbulence is generated by the source term $P_\mathrm{t}\langle \overline{p}_t\rangle$ and by the PBL scheme from turbulence shear production ($P_\mathrm{s}\langle \overline{p}_s\rangle$), the intensity of $P_\mathrm{t}\langle \overline{p}_t\rangle$ dominates over that of the shear production. The sum of the additional source term and the turbulence shear production, causes within the wind farms an increased turbulence from the lowest model level upwards.

We use the results from the actuator disk approach without rotation from Wu and Porté-Agel (2013), to obtain a qualitative impression of the structure of the turbulence field from a LES model within a wind farm. The actuator disk approach from their LES model is most similar to the drag approach in the mesoscale model. Their Fig. 5c shows that higher and lower turbulence intensities dominate around the upper and lower turbine blade tip. Also,

23

a positive and negative shear stress occur above and below hub-height (their Fig. 7c). This indicates that the shear in velocity dominates the turbulence production. Similar features are present in the TKE field from the EWP scheme, where the increased and decreased TKE above and below hub-height are in like manner caused by an enhanced and reduced turbulence shear production with respect to the neutral logarithmic velocity profile. Furthermore, Wu and Porté-Agel (2013) shows an upper wake edge at around 4.5 turbine hub-heights for 10 aligned wind turbines after 60 turbine diameters (their Fig. 12). They defined the wake edge at the point where the velocity reduction for a given height was 1 %. Similarly, the edge of the wake can be found from an increased TKE due to shear production. For the outermost contour in Fig. 8, we obtain a vertical wake extension of around 5 turbine diameters for the EWP scheme at 4.8 km downstream (equivalent to 60 turbine diameters). At the same distance, it is around 7 turbine hub-heights for the WRF-WF scheme.

The influence of the TKE field to the velocity profile is analysed in Fig. 9. It shows the velocity deficit profile $\Delta U_x/U_{0_h}$ $\Delta\langle\bar{u}_x\rangle/\langle\bar{u}_{0,h}\rangle$ for both schemes and all vertical resolutions. Here U_{0_h} $\langle\bar{u}_{0,h}\rangle$ denotes the free-stream velocity at hub-height. The velocity deficit is defined as $\Delta U_x(z) = U(z) - U_{\text{free}}(z)$, where $U_{\text{free}}(z)$ $\Delta\langle\bar{u}_x(z)\rangle = \langle\bar{u}(z)\rangle - \langle\bar{u}_{\text{free}}(z)\rangle$, where $\langle\bar{u}_{\text{free}}(z)\rangle$ is the free-stream velocity profile from the reference simulation and $U(z)$ $\langle\bar{u}(z)\rangle$ the velocity profile from the wind farm simulation. The free-stream velocities from the EWP and WRF-WF simulations were visually indistinguishable. We choose the second and third grid-cell within the wind farm (C2 and C3) and the second point behind the wind farm (C7) that corresponds approximately to the location of M6.

Figure 9a shows the velocity deficit profiles from the EWP and WRF-WF scheme from the L60 simulation. The profiles indicate a stronger diffusion in the WRF-WF scheme compared to that in the EWP scheme. This can be recognised by the vertical extension of the vertical deficit profile at C7, behind the wind farm.

For the EWP scheme (Fig 9b), we find a maximum velocity deficit at hub-height and symmetric features around the maximum for the L40 and L80 simulations. Also, results from LES simulations, wind tunnel experiments, and measurements (Vermeer et al., 2003; Wu and Porté-Agel, 2013; Iungo et al., 2013) have a maximum velocity deficit at hub-height

24

in the far turbine wake for a neutral ~~conditions~~ boundary layer. The profiles in Vermeer et al. (2003) (their Fig. 36) and in Wu and Porté-Agel (2013) (their Fig. 4) additionally show symmetric features around the maximum with a shape similar to the velocity profile of the EWP scheme. Figure 9b demonstrates the vertical resolution independence of the EWP scheme within the wind farm: the velocity deficits of the L40 and L80 simulations are almost identical. A small difference is found below hub-height in the wind farm wake.

With the WRF-WF scheme (Fig. 9c) the maximum velocity deficit is displaced vertically above hub-height, which reaches the upper wind turbine blade tip at mast M6 (C7). The dependency of WRF-WF scheme to the chosen vertical resolutions is weak; differences are found within the wind farm (C2, C3) above hub-height. Also, the profiles from the WRF-WF scheme show increased (area-averaged) velocities inside the wind farm at the lowest model level. The wind farm simulations from Wu and Porté-Agel (2013) (their Fig. 13) do not support this behaviour.

6 Discussion

We use wind farm parametrisations implemented in a mesoscale models to simulate the effect of wind farm wakes in areas on the order of hundreds of kilometres. However, the models have a limited horizontal resolution and hence the local processes within a wind farm remain unresolved. In the proposed parametrisation, we use the classical wake theory (Tennekes and Lumley, 1972) to describe the sub-grid-scale wake expansion. Compared to empirical fits from for example Xie and Archer (2014) and Zang et al. (2013), it offers the advantage that the wake expansion is described as a function of atmospheric stability. In this study, we have validated the approach for different wind speeds in a neutral atmospheric boundary layer. Its performance as a function of atmospheric stability, which requires information of the profiles, will be investigated in future. Wu and Porté-Agel (2013) found in their LES model results a sensitivity of the velocity reduction to the wind farm layout. In current implementations of wind farm parametrisations, all turbines within a grid-cell experience the same upstream velocity. Although these parametrisations are not meant to

25

estimate the local velocity field within the wind farm, differences in velocity reduction within the wind farm could affect the velocity in the wake of it.

~~In future~~ <u>Future</u> implementations ~~it can be possible to~~ <u>may</u> account for the local flow within the wind farm by using data from high resolution models, which can be input to the mesoscale model via a look-up table as suggested by Badger et al. (2013) and Abkar and Porté-Agel (2015). However, we have at the moment no measurement data in the wind farm wake to validate these approaches for different wind farm layouts. At the Horns Rev I wind farm, we were restricted to the geometry of met masts positions, which did not allow to study the sensitivity of the velocity field in the wind farm wake for additional wind direction sectors.

A fair comparison between the mesoscale model and long-term measurements can be realised in several ways. One method is to match the simulation period to that observed. By selecting corresponding time frames, one can then compare the fields of interest. The main disadvantage of this method is that errors in the background flow simulated by the mesoscale model also exist, which complicates the analysis. The second method is to sample the data and the model simulations in rather strict idealised conditions of wind speed and direction. We have chosen this second method using the WRF model in idealised case mode and compare its results to properly averaged measurements. Here the equilibrium solution without the wind farm effects is purposely made to match the free stream velocity and thus background errors in the simulations are absent. Besides a more detailed ~~analyses~~ <u>analysis</u>, this method also allows the study of the vertical dependency of the velocity reductions, since the atmospheric background conditions are almost identical for the simulations with ~~the~~ different vertical ~~resolution~~ <u>resolutions</u>.

Before we validated the results of the schemes in the wake of the wind farm, the a priori unknown initial length scale of the EWP scheme had to be determined. We did this using the turbine power measurements from the most frequently observed wind speed bin. This limitation could not be avoided, since to our knowledge no other long-term measurements from large offshore wind farms are available. <u>We found for the most frequently observed wind speed bin an initial length scale of $\sigma_0 = 1.7 r_0$ that fitted the turbine measurements the best.</u>

26

We recommend this constant for similar wind turbines. Future wind turbine measurements are needed to determine this value for other turbine types, such as low induction turbines. This constant was then used for the validation of all wind speed bins. On the other hand, for the WRF-WF scheme we have used the turbine specific thrust and power curves, which are its only input parameters. The difference of 0.1 % between the velocity deficit simulated by the WRF-WF and EWP scheme at the end of the wind farm for the $10\,\mathrm{m\,s^{-1}}$ wind speed bin, facilitated the comparison between the schemes in the wind farm wake, where the parametrisations are not active anymore.

One major difference between the EWP and WRF-WF approach is in the treatment of the grid-cell averaged TKE budget equation. The TKE production regulates the vertical profiles of momentum, temperature, and moisture within the PBL. Differences in TKE production would thus affect the local weather (e.g., temperature, humidity, and possibly clouds) response to the presence of large wind farms. ~~For the WRF-WF and EWP scheme , the PBL scheme adjusts the TKE production through the changed~~ Both wind farm schemes use a PBL scheme that parametrises the TKE equation in terms of grid-cell averaged variables. Therefore, in the wake of the wind turbines TKE is generated by the increased vertical shear in horizontal velocity. ~~The term that represents the local turbine-induced turbulence is neglected in the EWP approach, whereas it is parametrised as an additional source term~~ Then, the different definition of the unresolved velocity fluctuation in the WRF-WF and EWP scheme leads to a different term $\langle \overline{p}_t \rangle$ that is the direct consequence of the presence of a drag force. In the EWP scheme, a velocity fluctuation is defined around the ensemble-averaged velocity. With this definition $\langle \overline{p}_t \rangle$ is small and can be neglected. Instead, in the WRF-WF scheme. ~~. The~~ velocity fluctuations are defined around the grid-cell averaged velocity and a parametrisation of $\langle \overline{p}_t \rangle$ is added to the model TKE equation. The simulations have shown that in the WRF-WF scheme $\langle \overline{p}_t \rangle$ dominates over the shear production and that its total TKE is more than 3 times larger than that in the EWP scheme. However, it is unclear how well the actual grid-cell averaged shear production is approximated by the shear production calculated with the PBL scheme in WRF, on which the ~~in the WRF-WF scheme than in the~~ EWP scheme ~~. Future measurement campaigns~~

27

~~around large~~ relies. Therefore, future measurement campaigns of the actual structure and intensity of the TKE field within and around wind farms under suitable atmospheric conditions can help to settle this issue.

7 Conclusions

We introduce a wind farm parametrisation for use in mesoscale models. The EWP approach is based on classical wake theory and parametrises the unresolved expansion of the turbine-induced wake explicitly in the grid-cell that contains turbines, where the largest velocity gradients occur. The associated turbulence shear production is then determined by the PBL scheme in the mesoscale model. The approach has been implemented in the WRF mesoscale model and can be used with any PBL scheme. However, we recommend PBL schemes that model the TKE equation.

We analysed the results of simulations from the scheme in the wake of a wind farm. For the validation, we used the averaged wind speeds within a $30°$ wind direction sector at two met masts in the wake of the Horns Rev I wind farm. The model was run for several wind direction bins that cover those sampled in the observations. For each wind speed bin, we compared a wind direction averaged wind speed to the similarly averaged measurements. We found that for all 5 velocity bins, the velocity modelled with the EWP scheme agreed well with the met mast measurements 2 and 6 km downstream from the edge of the wind farm. The ~~bias was less than 0.15m, except for the 7mwind speed bin at mast M6, where it was around 0.23m~~ EWP scheme reproduces the wind farm wake within the standard deviation of the measurements.

To our knowledge, no long-term data-sets are available to validate the details of the vertical structure of the velocity deficit and turbulence in the wake of the wind farm. In a qualitative comparison, we found the vertical structure of the modelled TKE field to ~~agreed~~ agree with that of actuator-disk simulations by LES models (Wu and Porté-Agel, 2013), with an increased and decreased TKE around the upper and bottom rotor tip, respectively. The TKE field in the EWP scheme led to a symmetric velocity deficit profile around hub-height, sim-

28

ilar to velocity deficit profiles in Wu and Porté-Agel (2013); Vermeer et al. (2003). Also, the vertical wind farm wake expansion in the EWP approach was similar to that described in the before mentioned studies. While validation of the WRF-WF parametrisation has before been carried out with measurements within a wind farm (Jiménez et al., 2014), this is the first time that the validation has been done in the wake of a wind farm, at the scales the mesoscale model was designed to simulate.

Appendix: A

We use the notation and symbols of Raupach and Shaw (1982), with the exception that the ensemble average is used instead of the time average. The instantaneous velocity, u_i, can be decomposed in a spatial average with a fluctuation around it, $u_i = \langle u_i \rangle + u_i''$ and an ensemble average with a fluctuation, $u_i = \overline{u}_i + u_i'$. Figure Figure 1 illustrates the instantaneous velocity (grey line), as well as the spatial (red line) and ensemble-averaged (blue line) velocity in the vicinity of a wake.

We can decompose the total kinetic energy:

$$\frac{1}{2}\langle \overline{u_i^2} \rangle = \frac{1}{2}\langle \overline{u_i^2} \rangle + \frac{1}{2}\langle \overline{u_i'^2} \rangle \tag{1}$$

$$= \frac{1}{2}\langle \overline{u}_i \rangle^2 + \frac{1}{2}\langle \overline{u_i''^2} \rangle + \frac{1}{2}\langle \overline{u_i'^2} \rangle. \tag{2}$$

In Eq. (1), we applied an ensemble and spatial averaging to the kinetic energy and we have decomposed the ensemble-averaged kinetic energy in an average and fluctuating part. Here, $\frac{1}{2}\langle \overline{u}_i^2 \rangle$ is the spatial average of the ensemble-averaged kinetic energy and $\frac{1}{2}\langle \overline{u_i'^2} \rangle$ the spatial average of the kinetic energy from random velocity fluctuations.

29

By decomposing the first term on the r.h.s. of Eq. (1), we obtain Eq. (2). In Eq. (2), we now have three contributions to the total spatial and ensemble-averaged kinetic energy. The first term $\frac{1}{2}\langle\overline{u}_i\rangle^2$ is the kinetic energy of the spatial and ensemble-averaged velocity. The second term $\frac{1}{2}\langle\overline{u}_i''^2\rangle$ is the spatial-averaged kinetic energy of the heterogeneous part of the mean flow, which is the difference between the ensemble and spatial-averaged kinetic energy. This term arises only in non-homogeneous flow conditions and is also called "dispersive kinetic energy" by Raupach and Shaw (1982).

For each contribution on the r.h.s. of Eq. (2) to the total kinetic energy, a budget equation can be derived. The complete set of equations can for example be found in Raupach and Shaw (1982). We can combine the three components in Eq. (2) to kinetic energy of the mean flow (MKE) and turbulence kinetic energy (TKE). The MKE is not directly resolved by the model. However, the definition of TKE determines how the effect of wind turbines to the TKE is parametrised.

In approach I, one can define MKE $= \frac{1}{2}\langle\overline{u}_i^2\rangle = \frac{1}{2}\langle\overline{u}_i\rangle^2 + \frac{1}{2}\langle\overline{u}_i''^2\rangle$ and TKE $= \langle\frac{1}{2}\overline{u_i'^2}\rangle$ (Raupach and Shaw, 1982; Finnigan and Shaw, 2008). Here, the MKE is equal to the spatial average of the ensemble-averaged kinetic energy and it contains all kinetic energy of the organised motion. With this definition only random motion contributes to the TKE. The presence of the drag force gives rise to the term $\langle\overline{p}_t\rangle = \langle\overline{u_i'f_i'}\rangle$, where f' is the fluctuation of the drag force around the ensemble-averaged force. This approach is used in the EWP scheme and in Sect. 2.2 the additional term is derived.

In approach II, one could define MKE $= \frac{1}{2}\langle\overline{u}_i\rangle^2$ and then the TKE $= \frac{1}{2}\langle\overline{u}_i''^2\rangle + \frac{1}{2}\langle\overline{u_i'^2}\rangle$. In this case, the MKE contains only kinetic energy from the spatial-averaged velocity. Whereas, the TKE contains now also energy from the heterogeneous part of the mean flow additional to the energy from random motion. In this approach, a fluctuation can be decomposed in $u'' = \overline{u}_i'' + u_i'$. Therefore, the source term becomes $\langle\overline{p}_t\rangle = \langle\overline{u_i''f_i''}\rangle$, where

f'' is the fluctuation of the drag force around the spatial averaged-force. In the WRF-WF, this approach is used (see Sect. 4.1.2).

Appendix: B

In the EWP scheme, we approximate the velocity deficit profiles on the r.h.s. of Eq. (11), by a Gaussian shaped velocity profile on the l.h.s. of Eq. (11).

To show that these profiles are to a good approximation similar, we compare the difference between the average of 5000 single profile at distances $0 < x < 500\,\mathrm{m}$ to the approximated Gaussian velocity deficit. We normalise both profiles by the depth, Δy, of the wake in the cross-stream direction. For the comparison we used $U_0 = 8\overline{u}_0 = 8\,\mathrm{m\,s^{-1}}$, $R_0 = r_0 = 40\,\mathrm{m}$, $\sigma_0 = \sigma_0 = 60\,\mathrm{m}$, $C_T = c_T = 0.8$, $K = 6\,\mathrm{m^2\,s^{-1}}$, and $\Delta y = 1120\,\mathrm{m}$. The wake centre is defined at $z = 0\,\mathrm{m}$.

The result in Fig. 10 shows that the differences between the spatial averaged Gaussian profiles and the Gaussian profile with the space averaged spread is in the entire velocity deficit region far less than $0.001\,\mathrm{m\,s^{-1}}$.

Code availability

In this section a short guideline of the usage of the EWP scheme in the WRF model is given. The EWP approach can be run either in serial, shared-memory, or distributed memory options. Currently, it is not possible to run the approach with the mixed shared and distributed memory option. The scheme can be used for `idealised` and `real` case simulations. For the `real` case simulations, the wind farm parametrisation can be activated in any nest of the simulations. The additional namelist.input option `bl_turbine` should be used to select the wind farm parametrisation.

The EWP scheme needs additional input files in ASCII format. In the first file the positions and types of all wind turbines should be listed. The file name has to be specified as a string in the additional namelist.input option `windturbines_spec`. For every turbine used, the turbine characteristics, i.e., the hub-height and diameter, and the thrust and power coef-

ficients as a function of wind speed, need to be listed in a file. The power coefficient is used optionally to estimate the turbine power production. This file name has to start with the turbine type used in the first file, followed by the extension `.turbine`.

Please contact pvol@dtu.dk to obtain the code of the EWP wind farm parametrisation.

The Supplement related to this article is available online at doi:10.5281/zenodo.17109.

References

Abkar, M. and Porté-Agel, F.: A new wind-farm parameterization for large-scale atmospheric models, J. Renewable and Sustainable Energy, 7, 013121, doi:10.1063/1.4907600, 2015.

Adams, A. S. and Keith. D. W.: A wind farm parametrization for WRF, 8th WRF Users Workshop, 11–15 June 2007, Boulder, abstract 5.5, available at: http://www2.mmm.ucar.edu/wrf/users/workshops/WS2007/abstracts/5-5_Adams.pdf, 2007.

Badger, J., Volker, P. J. H., Prospathospoulos, J., Sieros, G., Ott, S., Rethore, P.-E., Hahmann, A. N., and Hasager, C. B.: Wake modelling combining mesoscale and microscale modelsm, in: Proceedings of ICOWES, Technical University of Denmark, 17–19 June 2013, Lyngby, p. 182–193, available at: http://indico.conferences.dtu.dk/getFile.py/access?resId=0&materialId=paper&confId=126, 2013.

Baidya Roy, S.: Simulating impacts of wind farms on local hydrometeorology, J. Wind Eng. Ind. Aerod., 99, 491–498, 2011.

Baidya Roy, S. and Traiteur, J. J.: Impact of wind farms on surface air temperature, P. Natl. Acad. Sci. USA, 107, 17899–17904, 2010.

Baidya Roy, S., Pacala, S. W., and Walko, R. L.: Can large wind farms affect local meteorology?, J. Geophys. Res., 109, 2156–2202, 2004.

5 Barrie, D. B. and Kirk-Davidoff, D. B.: Weather response to a large wind turbine array, Atmos. Chem. Phys., 10, 769–775, doi:10.5194/acp-10-769-2010, 2010.

Blahak, U., Goretzki, B., and Meis, J.: A simple parametrisation of drag forces induced by large wind farms for numerical weather prediction models, EWEC Conference, 20–23 April 2010, Warsaw, p. 186–189, available at: http://proceedings.ewea.org/ewec2010/allfiles2/757_
10 EWEC2010presentation.pdf, 2010.

Calaf, M., Meneveau, C., Meyers, J.: Large eddy simulation study of fully developed wind-turbine array boundary layers, Phys. Fluids, 22, 015110, doi:doi:10.1063/1.3291077, 2010.

Christiansen, M. B. and Hasager, C. B.: Wake effects of large offshore wind farms identified from satellite SAR, Remote Sens. Environ., 98, 251–268, 2005.

15 Crespo, A. and Hernández, J.: Turbulence characteristics in wind-turbine wakes, J. Wind. Eng. Ind. Aerod., 61, 71–85, 1996.

Finnigan, J. J. and Shaw, R. H.: Double-averaging methodology and its application to turbulent flow in and above vegetation canopies, Acta Geophysica, 56, 534-561, doi:10.2478/s11600-008-0034-x, 2008.

20 Fitch, A. C., Lundquist, J. K., and Olson, J. B.: Mesoscale influences of wind farms throughout a diurnal cycle, Mon. Weather Rev., 141, 2173–2198, 2013a.

Fitch, A. C., Olson, J. B., and Lundquist, J. K.: Parameterization of Wind Farms in Climate Models, J. Climate, 26, 6439–6458. doi:doi: http://dx.doi.org/10.1175/JCLI-D-12-00376.1, 2013b.

Fitch, A. C., Olson, J. B., Lundquist, J. K., Dudhia, J., Gupta, A., Michalakes, J., and Barstad, I.:
25 Local and mesoscale impacts of wind farms as parameterized in a mesoscale NWP model, Mon. Weather Rev., 140, 3017–3038, 2012.

Frandsen, S. T., Jørgensen, H. E., Barthelmie, R., Badger, J., Hansen, K. S., Ott, S., Rethore, P.-E., Larsen, S. E., and Jensen, L. E.: The making of a second-generation wind farm efficiency model complex, Wind Energy, 12, 445–458, 2009.

30 Gaumond, M., Réthoré, P.-E., Ott, S., Peña A., Bechmann, A., and Hansen, K. S.: Evaluation of the wind direction uncertainty and its impact on wake modeling at the Horns Rev offshore wind farm, Wind Energy, 7, 1169–1178, 2014.

Hahmann, A. N., Vincent, C. L., Peña, A., Lange, J., and Hasager, C. B.: Wind climate estimation using WRF model output: method and model sensitivities over the sea, Int. J. Climatol., published online, doi:10.1002/joc.4217, 2014.

Hansen, K. S., Barthelmie, R. J., Jensen, L. E., and Sommer, A.: The impact of turbine intensity and atmospheric stability on power deficits due to wind turbine wakes at Horns Rev wind farm, Wind Energy, 15, 183–196, 2012.

Hansen, M. O. L.: Aerodynamics of Wind Turbines, James & James, London, UK, 2003.

Hasager, C. B., Rasmussen, L., Peña, A., Jensen, L. E., and Réthoré, P.-E.: Wind farm wake: the Horns Rev Photo Case, Energies, 6, 696–716, 2013.

Iungo, G. V., Wu, Y.-T., and Porté-Agel, F.: Field measurements of wind turbine wakes with lidars, J. Atmos. Ocean. Tech., 30, 274–287, 2013.

Jacobson, M. Z. and Archer, C. L.: Saturation wind power potential and its implications for wind energy, P. Natl. Acad. Sci. USA, 109, 15679–15684, 2012.

Jiménez, P. A., Navarro, J., Palomares, A. M., and Dudhia, J.: Mesoscale modeling of offshore wind turbine wakes at the wind farm resolving scale: a composite-based analysis with the Weather Research and Forecasting model over Horns Rev, Wind Energy, 18, 559–566, 2014.

Keith, D. W., DeCarolis, J. F., Denkenberger, D. C., Lenschow, D. H., Malyshev, S. L., Pacala, S., and Rasch, P. J.: The influence of large-scale wind power on global climate, P. Natl. Acad. Sci. USA, 101, 16115–16120, 2004.

Lu, H., and Porté-Agel, F.: Large-eddy simulation of a very large wind farm in a stable atmospheric boundary layer, Phys. Fluids, 23, 065101, doi:doi:10.1063/1.3589857, 2011.

Nakanishi, M. and Niino, H.: Development of an improved turbulence closure model for the atmospheric boundary layer, J. Meteorol. Soc. Jpn., 87, 895–912, 2009.

Porté-Agel, F., Wu, Y.-T., Lu, H., and Conzemius, R. J.: Large-eddy simulation of atmospheric boundary layer flow through wind turbines and wind farms, J. Wind Eng. Ind. Aerod., 99, 154–168, 2011.

Raupach, M. R. and Shaw, R. H.: Averaging procedures for flow within vegetation canopies, Bound.-Lay. Meteorol., 22, 79–90, doi:10.1007/BF00128057, 1982.

Sathe, A., Gryning, S.-E., and Peña, A.: Comparison of the atmospheric stability and wind profiles at two wind farm sites over a long marine fetch in the North Sea, Wind Energy, 14, 767–780, 2011.

Skamarock, W., Klemp, J., Dudhia, J., Gill, D., Barker, D., Duda, M., Huang, X., Wang, W., and Powers, J.: A Description of the Advanced Research WRF Version 3, NCAR Technical note, Massachusetts, USA, 2008.

Tennekes, H. and Lumley, J. L.: A First Course in Turbulence, The MIT Pess, Boulder, USA, available at: http://www2.mmm.ucar.edu/wrf/users/docs/arw_v3.pdf, 1972.

Vermeer, L. J., Søensen, J. N., and Crespo, A.: Wind turbine wake aerodynamics, Prog. Aerosp. Sci., 39, 467–510, 2003.

5 Wang, C. and Prinn, R. G.: Potential climatic impacts and reliability of very large-scale wind farms, Atmos. Chem. Phys., 10, 2053–2061, doi:10.5194/acp-10-2053-2010, 2010.

Wu, Y.-T. and Porté-Agel, F.: Simulation of turbulent flow inside and above wind farms: model validation and layout effects, Bound.-Lay. Meteorol., 146, 181–205, 2013.

Wyngaard, J. C.: Turbulence in the Atmosphere, Cambridge Press, Cambridge, UK, 2010.

10 Xie, S., Archer, C.: Self-similarity and turbulence characteristics of wind turbine wakes via large-eddy simulation, Wind Energy (2014) doi:DOI: 10.1002/we.1792

Zhang, W., Markfort, C. D., and Porté-Agel, F.: Wind-Turbine Wakes in a Convective Boundary Layer: A Wind-Tunnel Study, Bound.-Lay. Meteorol. 146, 161–179, 2013 doi:DOI 10.1007/s10546-012-9751-4.

Table 1. Average wind speed at the reference turbine ($\overline{U}_{\text{ref}}\overline{u}_{\text{ref}}$) and frequency of the measurements at the met mast for all wind speed bins within the wind direction range 255–285°.

Wind speed bin (m s^{-1})	$\overline{U}_{\text{ref}}\ \overline{u}_{\text{ref}}$ (m s^{-1})	N_{obs} at M6–M7
7 ± 0.5	7.00	887
8 ± 0.5	7.95	933
9 ± 0.5	8.95	1097
10 ± 0.5	10.05	990
11 ± 0.5	11.05	729

Table 2. The WRF model configuration used in the simulations.

Number of grid-cells in the horizontal plane (nx, ny):	80, 40
Horizontal grid spacing (km):	1.12
Domain size in x, y, z (km):	89.6, 33.6, 15
Wind farm extension ($nx \times ny$):	5×5
Boundary condition:	OPEN
PBL scheme:	Nakanishi and Niino (2009)
Surface layer scheme:	MYNN Monin-Obukhov similarity theory
TKE advection:	Yes
Pert Coriolis:	Yes
Roughness length (m):	2×10^{-4}
Coriolis frequency (s^{-1})	1.2×10^{-4}

Table 3. Details of the WRF simulations.

Wind direction range ($°$):	258.75–281.25
Wind direction interval ($°$):	3.75
Wind speeds ($\mathrm{m\,s^{-1}}$):	7.0, 8.0, 9.0, 10.0 and 11.0
Number of vertical levels (nz):	40 (L40), 60 (L60), 80 (L80)
Wind farm parametrisation:	None, WRF-WF, EWP
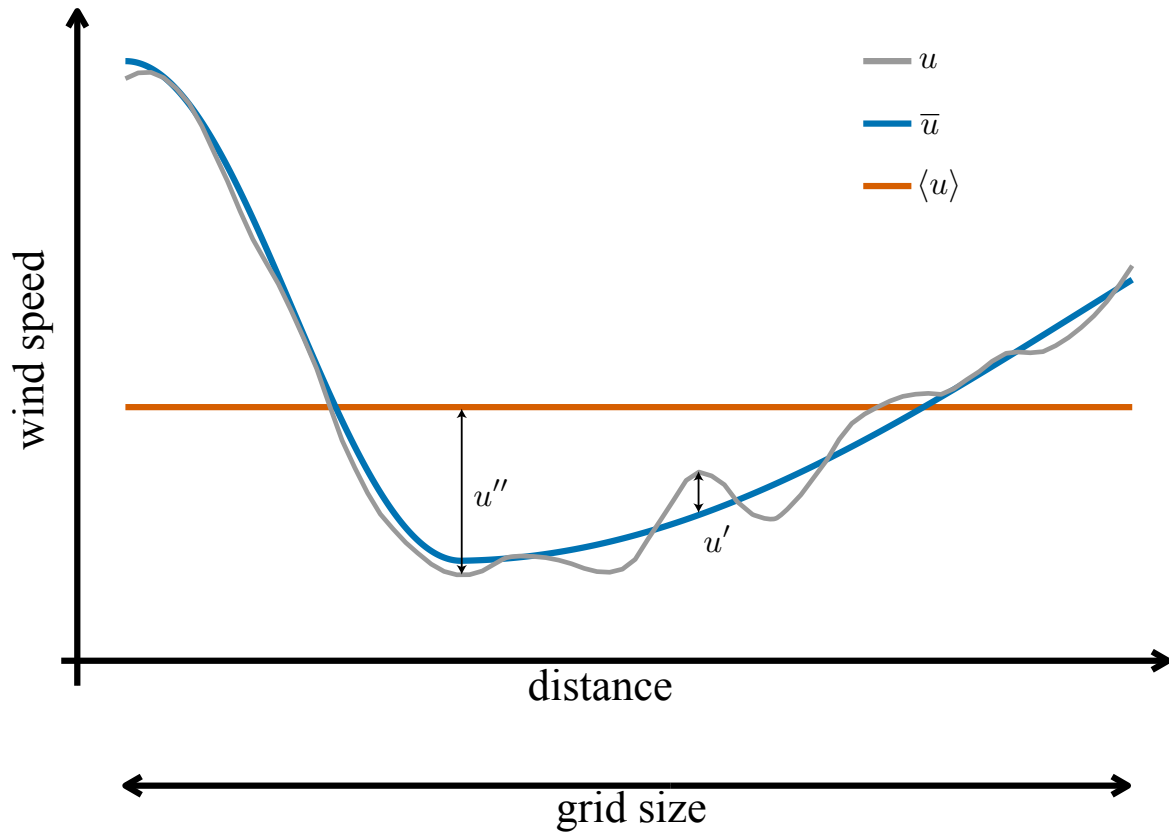
Figure 1. A sketch of the downstream development of a ~~-~~turbine induced velocity reduction~~for (a) the EWP scheme and (b) the WRF-WF scheme~~. ~~Δx~~ The x-axis indicates the grid-cell size. The ~~black lines represent the average for each approach and the~~ grey line represents the instantaneous velocity ~~$\widetilde{U}$. We used U for the ensemble-average velocity~~ and ~~$\langle U \rangle$ for~~ the ~~grid-cell~~ coloured lines the averaged ~~velocity~~ values. The difference between the average and instantaneous velocity defines the turbulence fluctuation at each distance~~x~~.
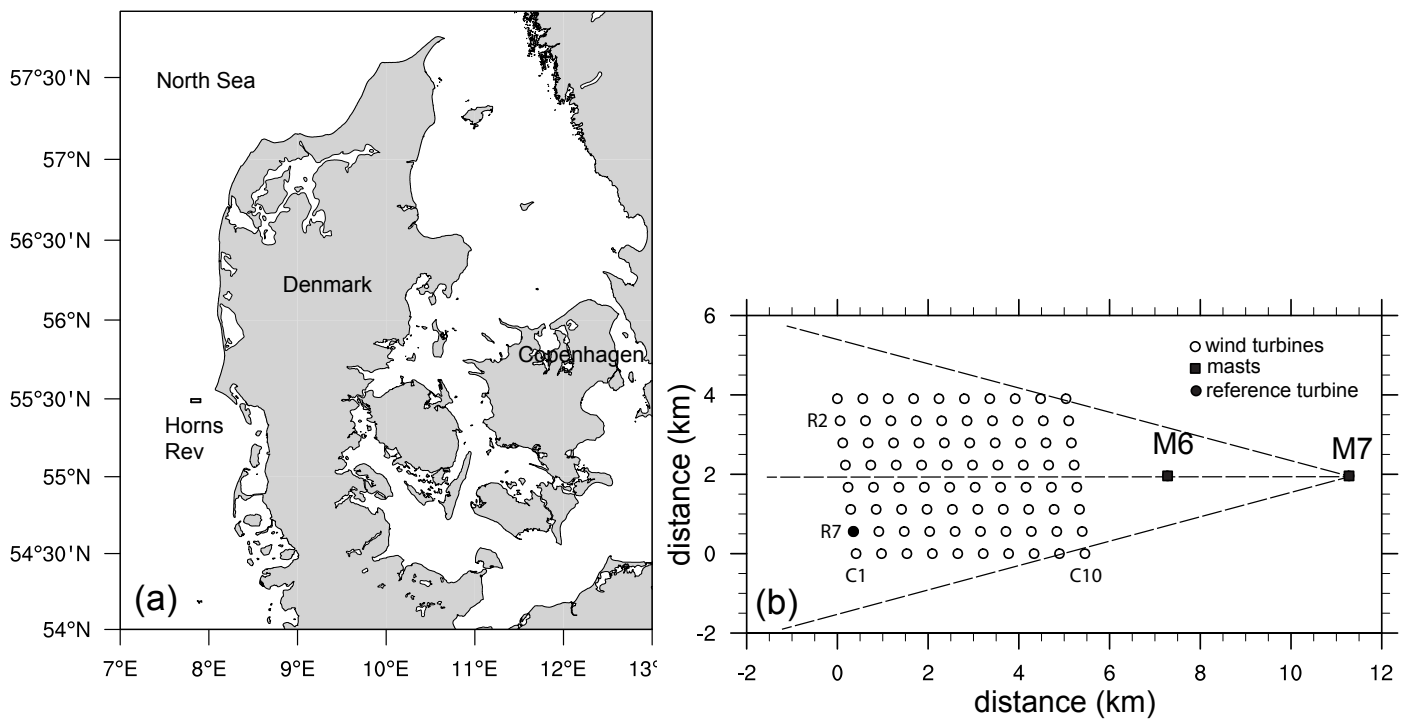
Figure 2. Location and layout of the offshore wind farm Horns Rev I including two nearby masts (M6 and M7). The centre of the wind farm and width of the sector ($\pm 15°$) used for the filtering of the measurements are indicated by the dashed lines.

(a)

$5\Delta x \times 5\Delta y$

(b)
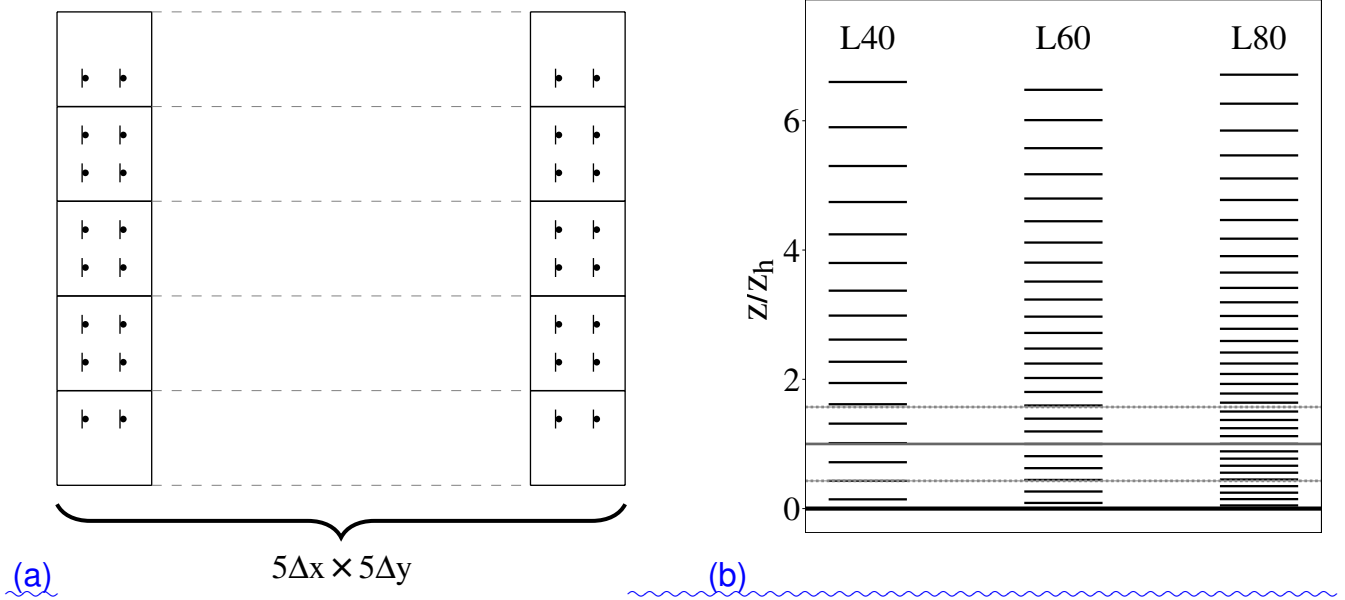
Figure 3. (a) Illustration of the model wind farm layout as applied in the mesoscale model. The squares indicate the model grid-cells and the wind turbines are marked with triangles. **(b)** Height (normalised by the turbine hub height) of the model mass-levels for the three simulations: L40, L60 and L80. The solid grey line and the dashed lines mark the hub-height and the upper and lower turbine blade tip, respectively.
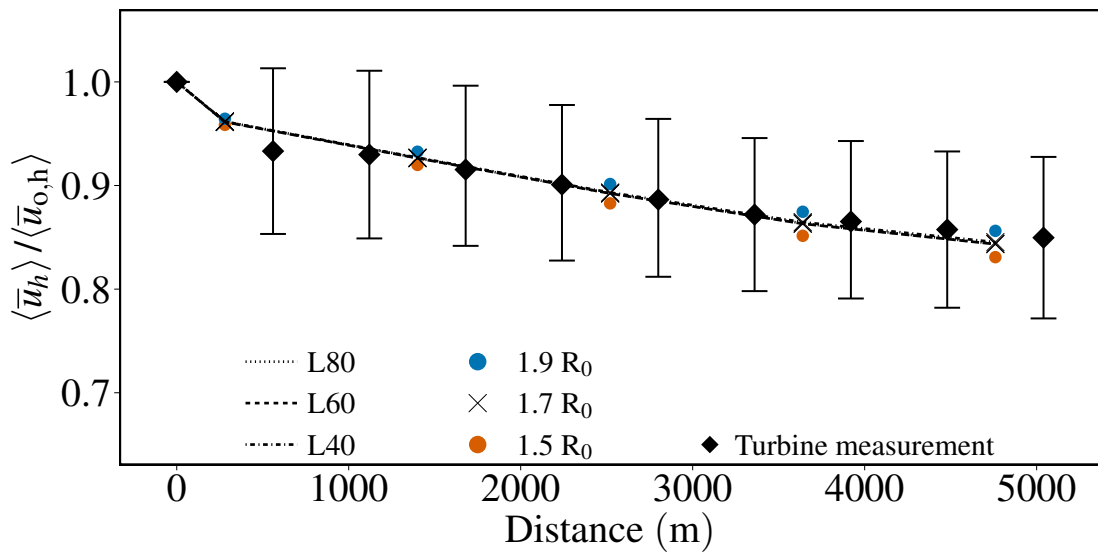
41

Figure 4. Measured and simulated hub-height velocity within the wind farm. The lines show the model simulated velocities averaged over wind direction with an initial length scale $\sigma_0 = 1.7 R_0$ $\sigma_0 = 1.7 r_0$ for the 3 vertical resolutions (L40, L60, and L80). The ~~dots~~ diamonds represent the measured turbine velocity averaged over each row and the bars indicate their standard deviations. The crosses mark the velocity at the grid-cell centre. The normalised velocity for $\sigma_0 = 1.5 r_0$ and $\sigma_0 = 1.9 r_0$ is shown with red and blue dots.

(a)

(b)
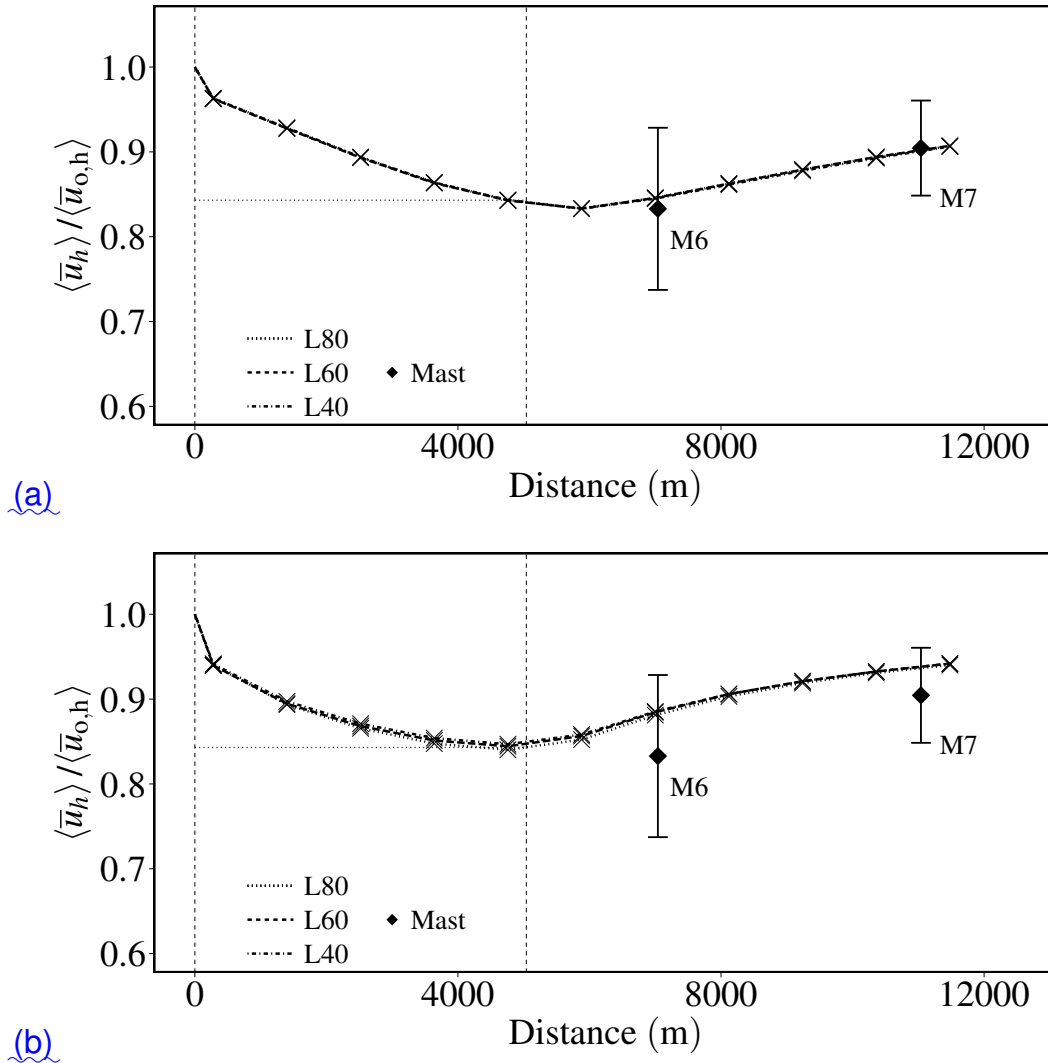
Figure 5. Hub-height velocity for the EWP **(a)** and WRF-WF **(b)** parametrisations for the L40, L60 and L80 simulations and observations as a function of distance from the western edge of the wind farm. The lines show the model simulated velocities, with the crosses showing the velocity at the grid-cell centre. The diamonds are used for the met mast measurements the bars their standard deviation. The vertical dashed lines show the wind farm extension and the horizontal dotted line the velocity with the EWP scheme at the easternmost grid-cell.
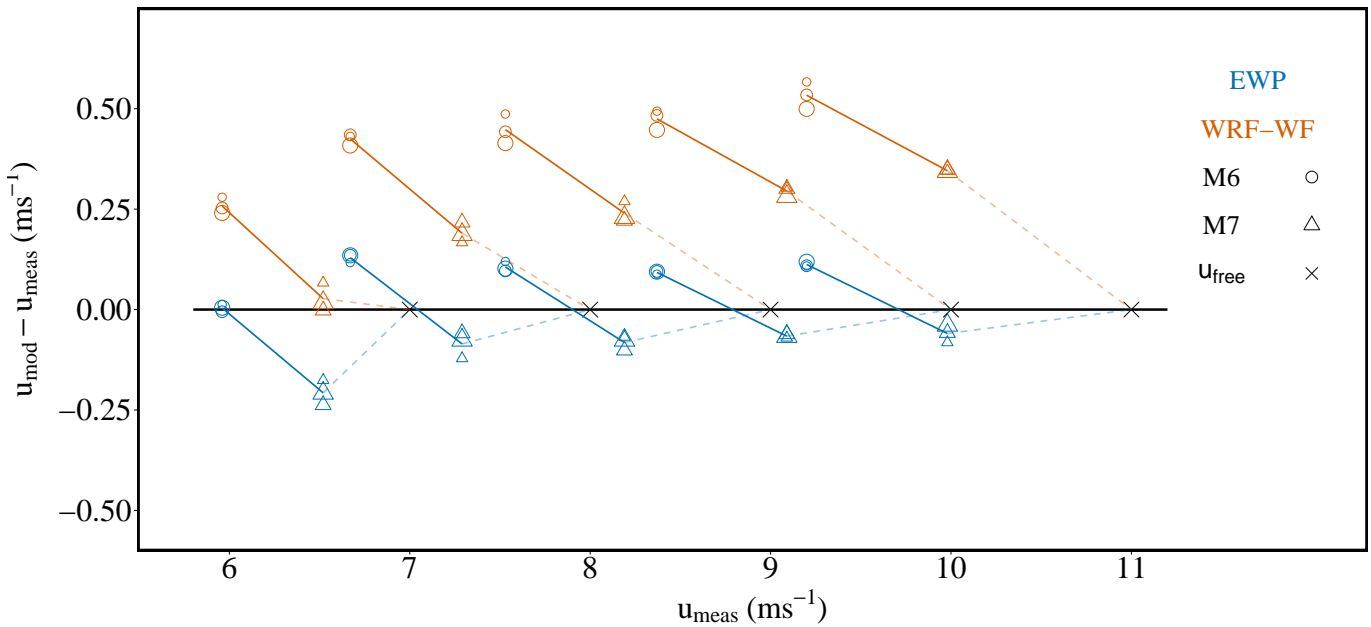
Figure 6. Modelled (U_{mod}) minus measured wind speeds (U_{meas}) at M6 (circles) and M7 (triangles) as a function of their measured wind speed, for the EWP (blue symbols) and the WRF-WF scheme (red symbols) for five wind speed bins and three vertical resolutions (symbol sizes). The coloured solid lines link the M6 and M7 values for the same wind speed bin, whereas the dashed lines the values from M7 and the free-stream velocities at the end of the wake. The crosses indicate the free-stream velocity.
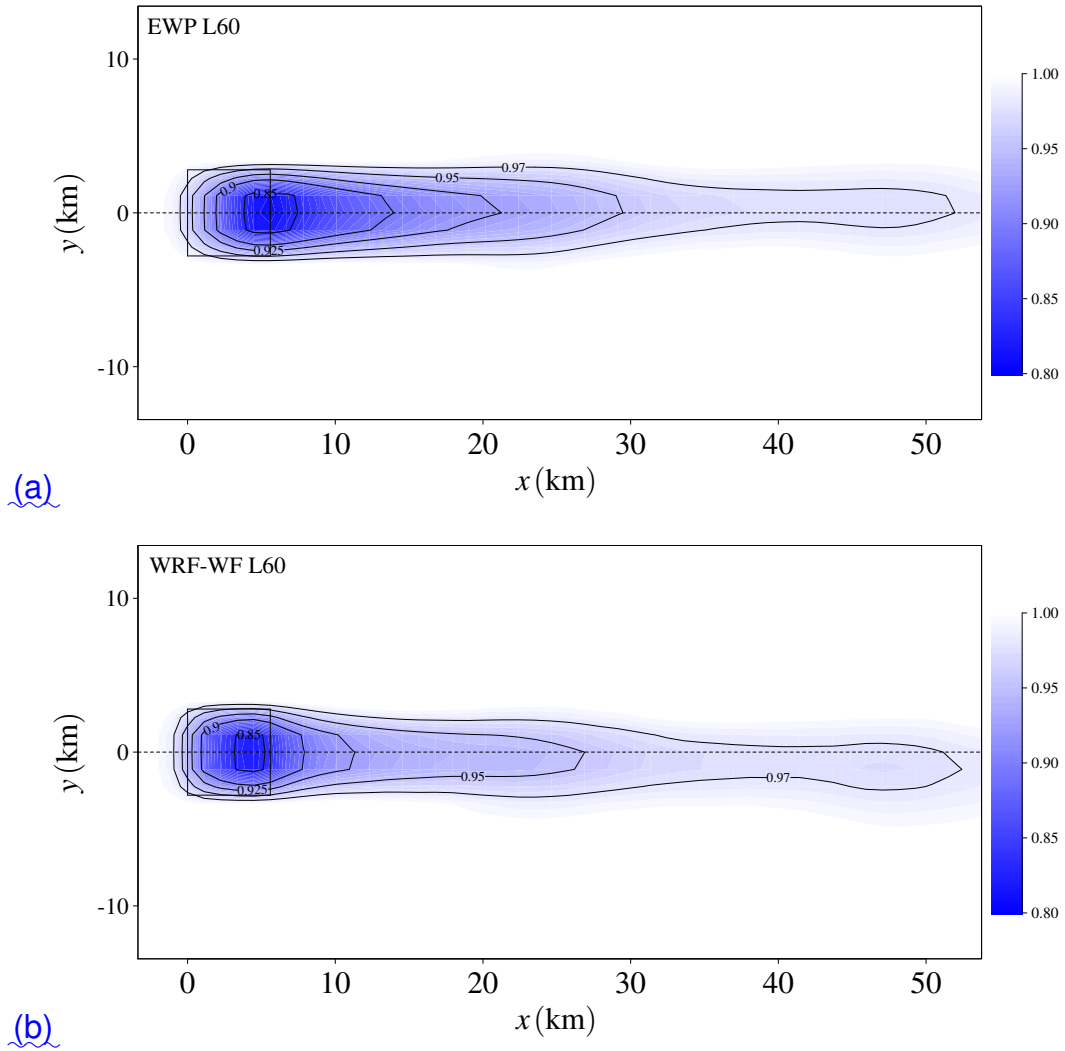
Figure 7. Horizontal view of the WRF-simulated velocity field at hub-height using the **(a)** EWP and **(b)** WRF-WF schemes. The simulations are for $10\,\mathrm{m\,s^{-1}}$ in the $270°$ wind direction and L60. The dotted line indicates the latitudinal centre and the solid rectangle the outer boundary of the wind farm.

(a)

(b)
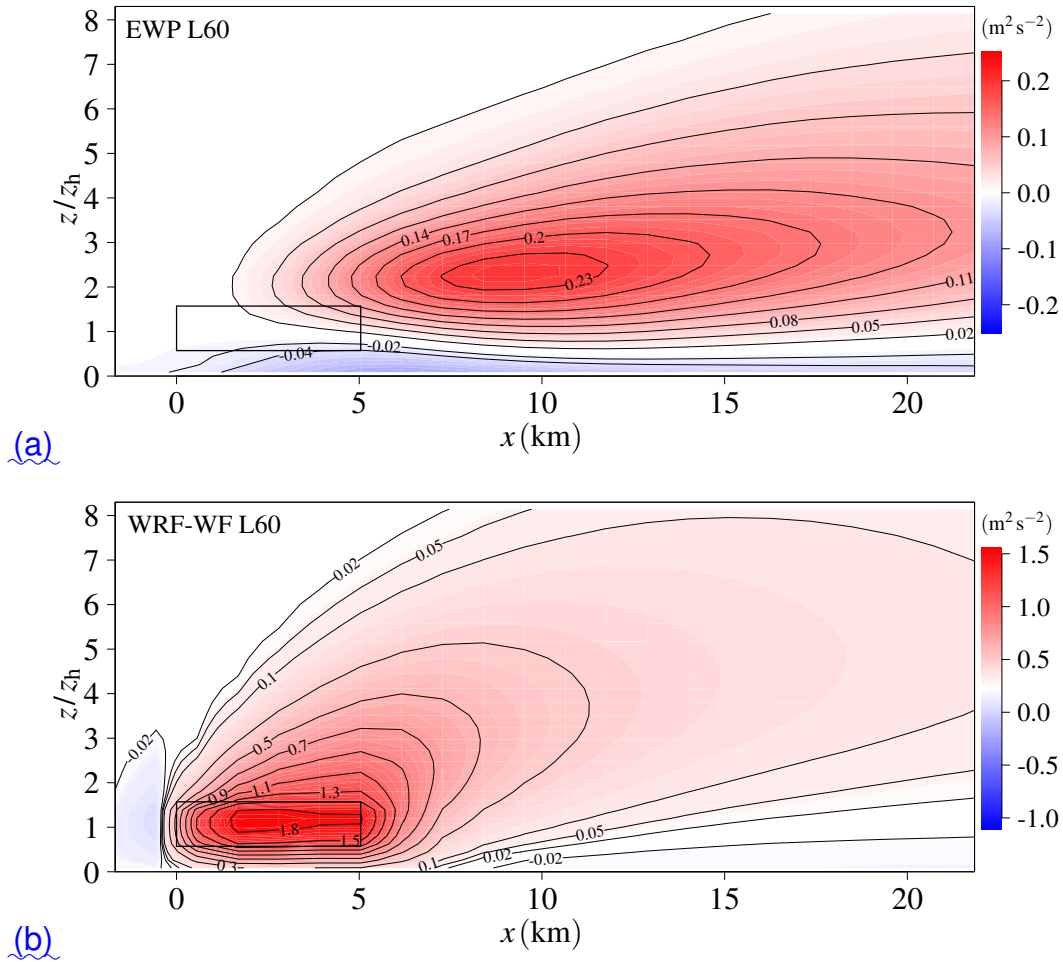
Figure 8. Vertical cross-section of the TKE difference ($\langle\bar{e}_{wf}\rangle - \langle\bar{e}_{ref}\rangle$) ($m^2\,s^{-2}$) for the simulations for $10\,m\,s^{-1}$ in the $270°$ wind direction and L60 for the **(a)** EWP and **(b)** WRF-WF scheme. The region in the model containing turbine blades is indicated by the rectangle.
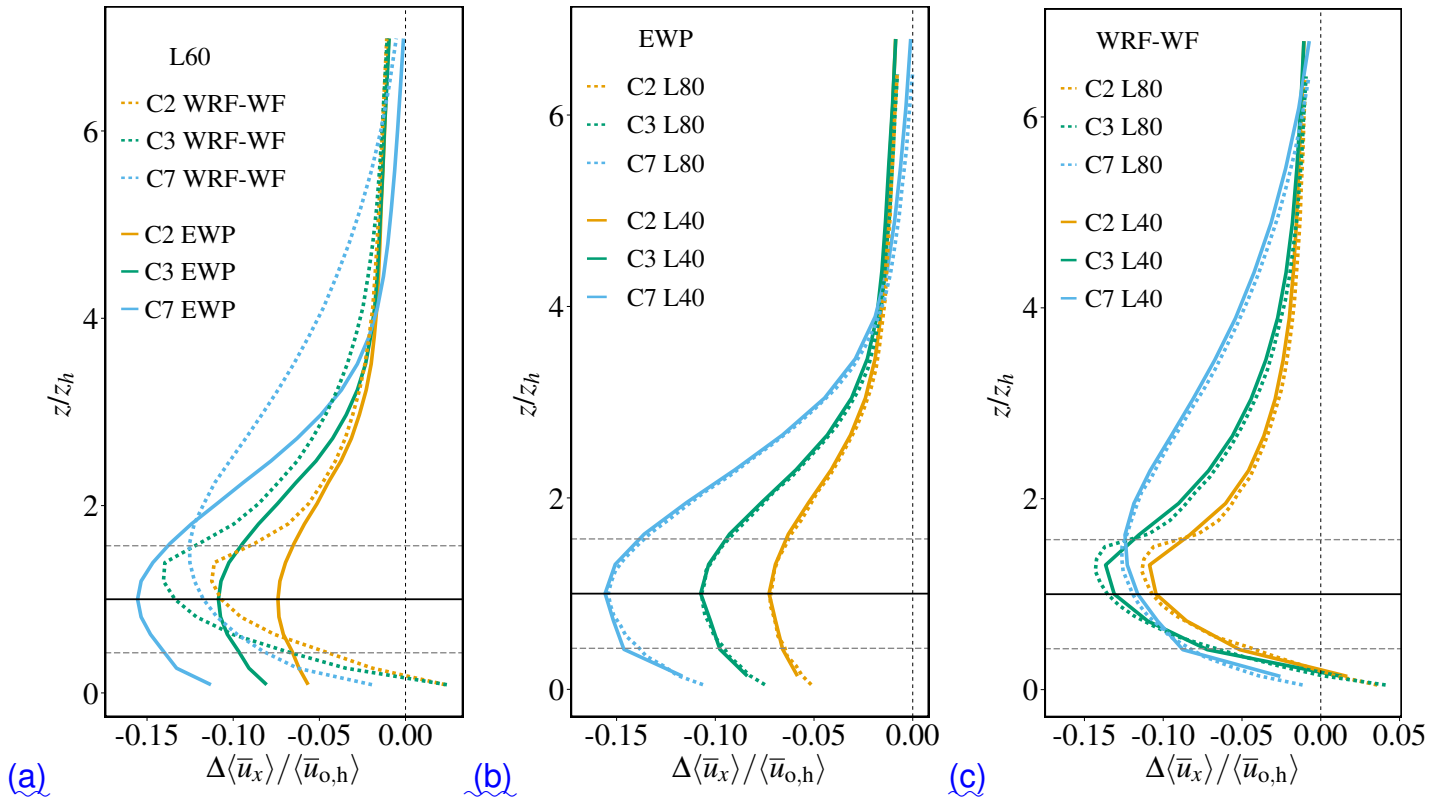
Figure 9. Comparison of the vertical profiles of simulated velocity deficit for the second (C2), third (C3) and seventh (C7) grid-cell containing wind turbines from the first westernmost turbine: **(a)** L60 simulations, **(b)** L40 and L80 simulation for the EWP, and **(c)** L40 and L80 simulation for the WRF-WF scheme. The turbine hub-height is indicated by the horizontal solid line and the turbine blade bottom and top by the dashed lines. The free-stream wind speed was $10\,\mathrm{m\,s}^{-1}$ in the $270°$ wind direction.
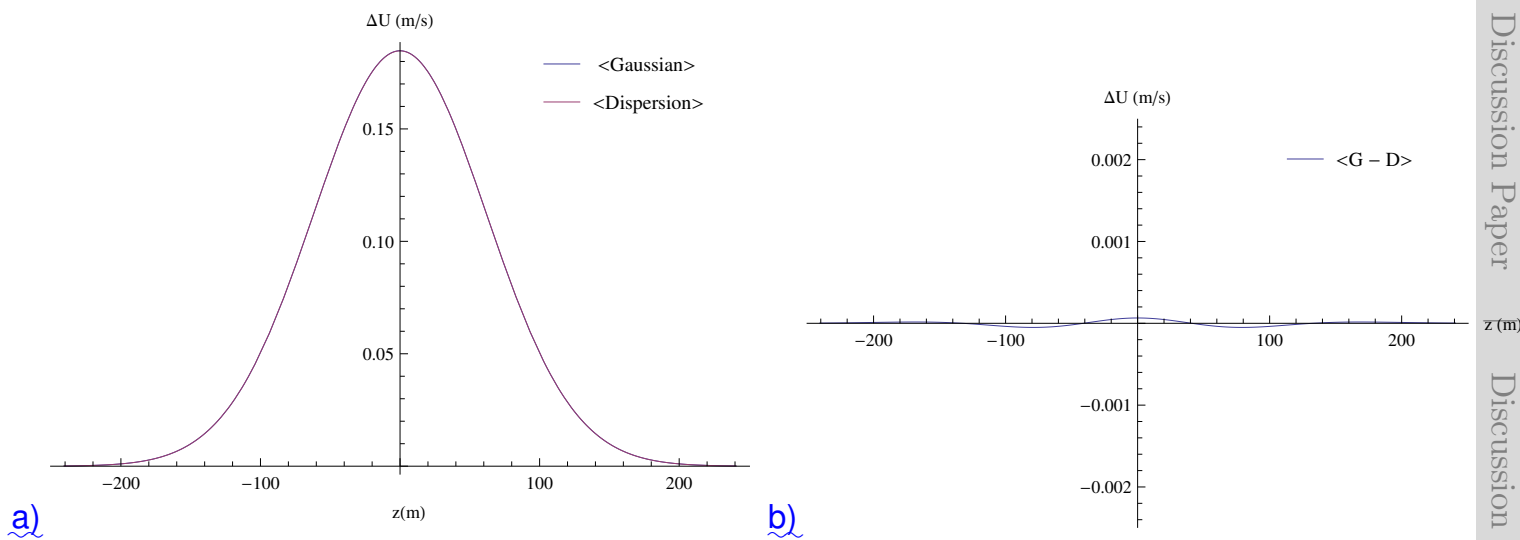
Figure 10. (a) shows a comparison between the distance average of the velocity deficit profiles (blue line) and the Gaussian profile with the average spread $\langle \sigma \rangle$ (red line). **(b)** shows the difference between the space averaged Gaussian profiles and the Gaussian profile with the average spread.